

**CHARACTERIZATION OF
ADIPOSITY-ASSOCIATED CHANGES
IN THE ADIPOSE TISSUE OF
PERIPARTAL DAIRY COWS**

by

Megan Lynn Clark

A thesis submitted to the Faculty of the University of Delaware in partial fulfillment of the requirements for the degree of Honors Bachelor of Science in Pre-Veterinary Medicine and Animal Biosciences with Distinction

Spring 2014

© 2014 Megan Lynn Clark
All Rights Reserved

**CHARACTERIZATION OF
ADIPOSITY-ASSOCIATED CHANGES
IN THE ADIPOSE TISSUE OF
PERIPARTAL DAIRY COWS**

by

Megan Lynn Clark

Approved: _____
Dr. Robert Dyer, VMD, Ph.D.
Professor in charge of thesis on behalf of the Advisory Committee

Approved: _____
Dr. Tanya Gressley, Ph.D.
Committee member from the Department of Animal and Food Sciences

Approved: _____
Dr. Nicole Donofrio, Ph.D.
Committee member from the Board of Senior Thesis Readers

Approved: _____
Michael Arnold, Ph.D.
Director, University Honors Program

ACKNOWLEDGMENTS

I would like to extend a huge thank you to Dr. Robert Dyer who made this entire project possible. As much as you'd like to debate the fact, you are the one who has taught me all that I know (to date) about research and the one who has made this entire project possible. Thank you for the countless hours of your time you donated, your unwavering patience and your infectious optimism. Most of all, thank you for bestowing the wonderful gift upon me which I will undoubtedly pass along to any and every young, upcoming student I get the chance to. I truly cannot thank you enough for all of the inspiration and encouragement you've given me over the years. I am so honored to have met and worked with you, and look forward to being a fellow colleague. Go Penn and go Quakers!

A special thank you goes out to Beth Morris who was a huge help in sizing countless adipocytes and getting this project to where it is now. Likewise, thank you to Amanda Barnard who helped to keep me sane in the lab, and who was there to make some (now comical) mistakes with me! Thank you to the Undergraduate Research Program for their generous, continued grant support and for making this Senior Thesis possible.

TABLE OF CONTENTS

LIST OF TABLES	vii
LIST OF FIGURES	viii
ABSTRACT	xii
1 INTRODUCTION	1
1.1 Defining adiposity	1
1.1.1 White adipose tissue: Functional compartments	1
1.1.1.1 Adipocytes	2
1.1.1.2 Stromal cell fraction	3
1.2 Murine and human models of adiposity and metabolic syndrome	4
1.2.1 Adipocyte hypertrophy vs. hyperplasia	4
1.2.1.1 Adipocyte hyperplasia	5
1.2.1.2 Adipocyte hypertrophy	7
1.2.2 T cell activation and dysregulation in adipose tissue	10
1.3 Adiposity in dairy cows	11
1.3.1 Industry standards to increase adiposity	11
1.3.2 Shift from lipogenesis to lipolysis at parturition	12
1.3.2.1 Blood metabolite elevations	13
1.3.3 Liver options for NEFA influx	13
1.3.4 Previous studies of bovine AT inflammation	15
1.3.5 Importance of research	16
1.3.6 Hypothesis and Objectives	17
2 MATERIALS AND METHODS	18
2.1 Materials	18

2.1.1	Reagents	18
2.1.2	Antibodies.....	19
2.1.3	Equipment.....	20
2.1.4	Supplies	20
2.2	Methods	20
2.2.1	Animal subjects	20
2.2.2	Adipocyte sizing.....	24
2.2.3	Lymph node crude cell fraction isolation	25
2.2.4	Adipose tissue SCF isolation.....	26
2.2.4.1	Collagenase preparation	26
2.2.4.2	Adipose tissue SCF isolation.....	26
2.2.5	Staining for flow cytometry.....	27
2.2.6	Fluorescence Activated Cell Sorting (FACS) analysis	28
3	RESULTS.....	31
3.1	Adipocyte area and BCS	31
3.2	Adipocyte size across tissue depots.....	34
3.3	Frequency distribution of adipocyte area	37
3.4	Immune cell infiltrates in mesenteric adipose tissue	40
3.4.1	LN population characteristics.....	40
3.4.2	ASCF population characteristics	41
3.4.3	Gating controls	42
3.4.4	CD11b.....	45
3.4.5	CD172.....	46
3.4.6	CD3.....	47
3.4.7	CD11b and CD172	48
3.4.8	CD11b and CD3	51
3.4.9	Mesenteric LN immune cell infiltrate profile.....	53
3.4.10	Mesenteric ASCF immune cell infiltrate profile	54
4	DISCUSSION.....	56
4.1	Adipocyte area and BCS	56
4.2	Adipocyte area by tissue depot.....	60
4.3	Characterizing immune cell infiltrates	60
4.3.1	Mesenteric lymph node	60
4.3.2	Adipose stromal cell fraction.....	61

4.4	Conclusions	65
4.5	Future areas of research.....	66
	REFERENCES	68

LIST OF TABLES

Table 1: Monoclonal primary antibodies employed to immunophenotype AT macrophages and lymphocytes in bovine ASCF and lymph node crude cell fraction (Bill Davis, Washington State University School of Veterinary Medicine, Monoclonal Antibody Center, Pullman, WA, USA) and corresponding fluorescent-conjugated secondary antibodies (Jackson ImmunoResearch, West Grove, PA, USA)	19
Table 2: Body condition score scale from 1-5 adapted from Penn State Body Condition Scoring System (Heinrichs et al., 1989, http://extension.psu.edu/animals/dairy/nutrition/nutrition-and-feeding/body-condition-scoring , 2004)	22

LIST OF FIGURES

Figure 1. Underweight cow, BCS=2.25. Visible hooks and pin bones with a V-shaped thurl. Backbone prominent; can easily see transverse lumbar processes.....	23
Figure 2. Overweight cow, BCS=4.5. Hooks and pins not visible, U-shaped thurl, rounded back, cannot discern transverse lumbar processes.	24
Figure 3. Mesenteric adipocyte cross-sectional area (μm) of 20 randomly selected adipocytes from a randomly selected field (100X).	25
Figure 4. Demonstration of adjustment of compensation for a single color FITC (FL-1) stained set of lymph node cells (stained for CD3). The left picture demonstrates an undercompensated set of cells without enough fluorescence subtraction. The PE median fluorescence intensity of the positive FITC population is greater than that of the negative FITC population. The figure on the right shows proper compensation where the median of the positive and negative FITC population is equal within the PE channel (“Technical Bulletin,” 2009).....	30
Figure 5. Level of adiposity (body condition) is directly correlated to mean mesenteric cross-sectional adipocyte area (μm^2) in bovine mid-jejunum mesenteric adipose tissue ($r=0.85$) ($n=16$).	32
Figure 6. Level of adiposity (body condition) is directly correlated to mean omental cross-sectional adipocyte area (μm^2) in bovine omental adipose tissue ($r=0.87$) ($n=15$).	33
Figure 7. Level of adiposity (body condition) is weakly correlated to mean subcutaneous cross-sectional adipocyte area (μm^2) in bovine subcutaneous adipose tissue ($r=0.59$) ($n=12$).	34
Figure 8. Mean mesenteric adipocyte area (μm^2) was directly correlated ($r=0.92$) with mean omental adipocyte area (μm^2) ($n=15$).	35
Figure 9. Mean mesenteric adipocyte area (μm^2) was directly correlated ($r=0.89$) with mean subcutaneous adipocyte area (μm^2) ($n=11$).	36

Figure 10. Mean omental adipocyte area (μm^2) was directly correlated ($r=0.92$) with mean subcutaneous adipocyte area (μm^2) (n=11).	37
Figure 11. Increased level of adiposity (body condition) shifts the frequency of mesenteric adipocyte cross-sectional area (μm) toward larger cell sizes in lean (BCS 1.5 (n=5), 2.5 (n=2)) and heavy (BCS 3.5 (n=2)) dairy cows.....	38
Figure 12. Increased level of adiposity (body condition) shifts the frequency of omental adipocyte cross-sectional area (μm) toward larger cell sizes in lean (BCS 1.5 (n=2), 2.5 (n=3)) and heavy (BCS 3.5 (n=1), 4.5 (n=1)) dairy cows.....	39
Figure 13. Increased level of adiposity (body condition) shifts the frequency of subcutaneous adipocyte cross-sectional area (μm) toward larger cell sizes in lean (BCS <2.0 (n=5), 2.0-3.0 (n=5)) and heavy (BCS >3.5 (n=2)) dairy cows.	40
Figure 14. Cytogram of lymph node crude cell fraction cells circled within the gate labeled “R1”. Forward scatter (FSC) and side scatter (SSC) of light from cells were measured by a FACSCalibur flow cytometer and gated cells were analyzed for fluorescence.	41
Figure 15. Cytogram of the mesenteric adipose stromal cell fraction circled within the gate. Forward scatter (FSC) and side scatter (SSC) of light from cells were measured by a FACSCalibur flow cytometer and gated cells were analyzed for fluorescence.....	42
Figure 16 Representative sample of double negative control lymph node crude fraction (A) and adipose stromal cell fraction (B) cells stained with both FITC and PE conjugated secondary antibodies, no primary antibody stain. Quadrant gates were established through analyzing secondary only stain after adjusting for single color stain compensation levels.	43
Figure 17. Representative quadrant statistics for control cells stained with secondary antibodies only. Red circles highlight the intentional 1% of cell events falling in the UL and LR quadrants with over 97% of gated events in the LL quadrant.....	44
Figure 18. Representative sample of unstained LN crude cell fraction (A) and unstained ASCF (B) for verification of gates set from cells stained only secondary antibodies.	45

Figure 19. Representative sample of CD11b+ macrophages, dendritic cells, and CD8+ effector T lymphocytes comprise $24.9\% \pm 2.47$ (mean \pm SEM) (n=6) of the LN crude cell fraction (A) and $12.7\% \pm 4.3$ (n=3) of the ASCF (B) as seen in cells positively emitting PE fluorescence in the UL quadrants. 46

Figure 20. Representative sample of CD172+ macrophages, dendritic cells, and monocytes comprise $6.4\% \pm 0.9$ (mean \pm SEM) (n=6) of the LN crude cell fraction (A) and $14.8\% \pm 8.7$ (n=3) of the ASCF (B) as seen in cells positively emitting FITC fluorescence in the LR quadrants. 47

Figure 21. Representative sample of CD3+ T lymphocytes comprise $77.9\% \pm 3.5$ (mean \pm SEM) (n=6) of the LN crude cell fraction (A) and $7.9\% \pm 1.1$ (n=3) of the ASCF (B) as seen in cells positively emitting FITC fluorescence in the LR quadrants. 48

Figure 22. Representative sample of CD11b and CD172 double stained LN crude cell fraction (n=7) (A) containing primarily CD11b+/CD172- monocytes, macrophages, CD8+ lymphocytes and dendritic cells and CD11b+/CD172+ macrophages and ASCF (n=3) (B) containing primarily CD11b+/CD172- monocytes, macrophages, lymphocytes and dendritic cells and CD11b-/CD172+ macrophages. 50

Figure 23. Mesenteric lymph nodes (n=7) contained CD11b+/CD172- macrophages, monocytes and/or dendritic cells, CD11b+/CD172+ macrophages, and CD11b-/CD172+ macrophages. Mesenteric adipose SCF (n=3) contained CD11b+/CD172- macrophages, monocytes and/or dendritic cells, CD11b+/CD172+ macrophages, and CD11b-/CD172+ macrophages. Note these early results showed the single positive CD172 macrophage fractions in the SCF may be higher in mesenteric adipose depots compared to the mesenteric lymph nodes. Data expressed as mean \pm SEM 51

Figure 24. Representative sample of CD11b and CD3 double stained LN crude cell fraction (n=2) (A) containing primarily CD11b-/CD3+ lymphocytes and CD11b+/CD3+ T lymphocytes and ASCF (n=3) (B) containing primarily CD11b+/CD3- monocytes, macrophages and dendritic cells and CD11b-/CD3+ T lymphocytes..... 52

Figure 25. Mesenteric lymph nodes (n=2) contained CD11b+/CD3- macrophages, monocytes and/or dendritic cells, CD11b+/CD3+ T lymphocytes, and CD11b-/CD3+ T lymphocytes. Mesenteric adipose SCF (n=2) contained CD11b+/CD3- macrophages, monocytes and/or dendritic cells, CD11b+/CD3+ lymphocytes, and CD11b-/CD3+ lymphocytes. Note the double positive cell fractions in the SCF were nearly nonexistent compared to the levels in the lymph node. Data expressed as mean±SEM..... 53

Figure 26. Mesenteric lymph node crude cell fraction contains 24.9%±2.47 (X±SEM) CD11b+ macrophages/dendritic cells (n=6), 6.4%±0.9 CD172+ macrophages (n=6), and 77.9%±3.5 CD3+ T lymphocytes (n=3). Data expressed as mean±SEM. 54

Figure 27. Mesenteric adipose stromal cell fraction (n=3) contains 12.7%±4.3 CD11b+ macrophages/dendritic cells, 14.8%±8.7 CD172+ macrophages, and 7.9%±1.1 CD3+ T lymphocytes. Data expressed as mean±SEM. 55

ABSTRACT

Modern nutritional programs in the dairy industry have been designed to increase adiposity during late lactation. Energy stored as fat is subsequently mobilized to support deep nadirs in lactational energy drain in the next lactation. Human and murine obesity models showed nutrient overburdened adipose tissues developed adipocyte hypertrophy and increased inflammatory and immune cell infiltration that led to inflammation (metabolic inflammation). Very little is known about the implications of increasing adipose tissue mass on metabolic inflammatory disorders in dairy cattle even though insulin resistance, dyslipidemia, and steatohepatosis are associated with heavy lactation. Accordingly, the purpose of this study was to begin to relate adipocyte area and immune cell infiltrates in bovine adipose tissue to adiposity. We hypothesized that bovine adipocytes expand in size (hypertrophy) in direct proportion to increased states of adiposity, and that immune and inflammatory cells exist as endogenous inhabitants of these adipose depots. Tissues were collected from mesenteric, omental, and subcutaneous adipose tissue (AT) depots of lactating Holstein dairy cows. Tissues were either fixed, stained and mounted to measure adipocyte size, or digested for isolation of the AT stromal cell fraction (ASCF). Isolated mesenteric ASCF cells, along with mesenteric lymph nodes (positive control), were fixed and stained for flow cytometric analysis. Mean mesenteric and omental adipocyte sizes increased in direct proportion ($r=0.85$, $r=0.87$) to body condition score (BCS) indicating hypertrophy, whereas mean subcutaneous adipocyte area was weakly correlated with BCS ($r=0.59$). Moreover, adipocyte hypertrophy caused a shift in the

frequency distribution of adipocyte size toward larger cell sizes. Mesenteric ASCF contained $12.7\% \pm 4.3$ CD11b+ macrophages/dendritic cells, $14.8\% \pm 8.7$ CD172+ macrophages, and $7.9\% \pm 1.1$ CD3+ T lymphocytes on average (n=3). These data indicated that dairy cows respond to nutrient burdens with hypertrophic responses in adipocytes across mesenteric and omental adipose tissue, parallel to adipocyte responses in human and murine models of obesity. Likewise, the results suggested that subcutaneous adipose tissue (SAT) was a highly variable depot which was not as closely regulated as visceral adipose tissue. FACS analysis of mesenteric ASCF showed that endogenous populations of T lymphocytes and macrophages/dendritic cells exist in the mesenteric adipose tissue. Collectively, the data suggests immune functions may impact metabolic homeostasis in bovine visceral adipose depots.

Chapter 1

INTRODUCTION

1.1 Defining adiposity

Adiposity is defined as the fraction of total body mass residing in adipose tissue mass. In bovines, white adipose tissue is divided into visceral adipose tissue (VAT) surrounding the organs and subcutaneous adipose tissue (SAT) depots lying underneath the skin. In addition to VAT and SAT depots, adipose tissue accompanying the mammary gland comprises a large amount of total body adipose, especially in lactating bovines. Mesenteric adipose, the deepest VAT depot, suspends the intestines in the abdomen in a web-like manner and is found in abundance around the jejunum. A second visceral adipose tissue depot is omental adipose, which begins at its attachment to the stomach and spleen and expands over the ventral abdomen, lying superficial to the mesentery. Subcutaneous adipose tissue lies beneath the skin, with larger depots localized around the tailhead, backbone, hook and pin bones, and over the rectus abdominis muscles in bovines.

1.1.1 White adipose tissue: Functional compartments

Although white adipose tissue was once viewed as solely an energy storage organ, various studies have illuminated its functions as one of the most important endocrine organs in the body (Daniel et al., 2003, Suganami et al., 2012). Adipose tissue is comprised of both the adipocyte parenchyma and the adipose stromal cell fraction (ASCF) interspersed between the adipocytes.

1.1.1.1 Adipocytes

Adipocytes are the endemic cell type of adipose tissue, making up the parenchyma of the tissue. Adipocytes are lipid droplets which have coalesced together into a lipid vesicle to internalize triglycerides, the storage form of fat. As a major energy source, triglycerides (TGs) have a 3 carbon sugar backbone (glycerol) with three 18-22 carbon long fatty acid chains covalently linked via ester bonds to the glycerol backbone. TGs are formed from metabolic intermediates (glycerol) derived from glucose metabolism and long chain fatty acids (LCFAs). The LCFAs are derived by absorption and digestion of exogenous sources like dietary fat or endogenous sources such as fat mobilized from adipose or hepatic tissues. Adipocytes synthesize and subsequently store TGs in large cytoplasmic fat vesicles. Ongoing TG synthesis and storage leads to progressive distention of the cytoplasmic fat vacuole, compression of the nucleus to one side of the cell, and over distention of the plasma membrane. The primary metabolic function of an adipocyte is to serve as a storage unit for triglycerides. TGs are mobilized from fat vesicles under states of heavy activation of the sympathetic nervous system or during acute or chronic states of negative energy balance.

Along with energy storage, adipocytes play a major functional role in the crosstalk between endocrine and immune systems. Being that endocrine communication is necessary for adipose tissue to remain in constant equilibrium with the body's energy state, heavy vascularization in the adipose tissue provides a vehicle for this communication. Adipocytes secrete factors, known as adipokines, which have a variety of cell signaling effects across a variety of organ systems. Adipokines can have effects on the hypothalamus to signal satiety (leptin), the vasculature to recruit immune cells (MCP-1), the surrounding tissue to create a pro-inflammatory

environment and activate macrophages (TNF- α), the adipocytes to regulate glucose uptake and fatty acid metabolism (adiponectin), and many other organ systems in through their various endocrine functions. Pro-inflammatory signals generated by adipocytes support insulin resistance, lipolysis and suppression of preadipocyte development. On the contrary, anti-inflammatory signals favor lipogenesis, preadipocyte progenitor cell activity and expansion, and insulin sensitivity. This wide range of functional effects demonstrates the crucial role of adipokines in maintenance or perturbation of adipose tissue homeostasis.

1.1.1.2 Stromal cell fraction

The adipose stromal cell fraction (ASCF) is comprised of cells such as preadipocytes, fibroblasts, endothelial cells, and neutrophils along with resident anti-inflammatory lymphocytes, monocytes and macrophages (Suganami et al., 2012). In normal adipose tissue, resident alternatively activated (M2) macrophages are present to control inflammation and secrete anti-inflammatory cytokines along with T regulatory lymphocytes, which secrete IL-10 and TGF- β to maintain homeostasis in the adipose tissue. The stromal cell fraction in healthy murine models is comprised of 10-20% macrophages (primarily M2, anti-inflammatory phenotypes). The anti-inflammatory milieu created by these endogenous immune cell inhabitants is critical to keep adipocytes in a lipogenic, insulin sensitive state. In states of adipose tissue inflammation, however, pro-inflammatory macrophages can make up 50-60% of the ASCF cell population (Weisberg et al., 2003). When pro-inflammatory, M1-polarized macrophages overwhelm the ASCF, they oppose phenotypic functions of M2 macrophages, therefore supporting lipolysis, blocking preadipocyte cell formation, and supporting insulin resistance in adipose tissues. Overall, local states of inflammation

in the adipose tissue are determined and controlled by the balance between pro-inflammatory and anti-inflammatory immune phenotypes.

1.2 Murine and human models of adiposity and metabolic syndrome

1.2.1 Adipocyte hypertrophy vs. hyperplasia

As adiposity increases adipocytes have two functional options available to promote storage of triglycerides; adipocytes can employ hypertrophy, an increase in cell size, or hyperplasia, an increase in cell number. Morbidly obese humans and mice responding to increased triglyceride burdens with hyperplastic responses maintain a normal, non-inflamed, insulin sensitive adipose tissue phenotype. On the other hand, adipocyte hypertrophy is an event preceding adipose tissue inflammation which has been linked to increased macrophage infiltrates in murine adipose tissue (Weisberg, 2003). Therefore, hyperplastic responses are deemed healthy methods of fat storage while hypertrophic responses are regarded as the unhealthy alternative mechanism of fat storage. In human and murine models of obesity and metabolic syndrome, adipocytes tend to shift toward a hypertrophic, rather than a hyperplastic phenotype, where individual adipocytes expand to accommodate greater triglyceride loading. Some previous data showed hyperplastic or hypertrophic responses to nutrient overloading may be controlled genetically. Animals responding through hypertrophic mechanisms trigger the pro-inflammatory sequella that results in a sterile, sustained and unresolving inflammatory reaction in the adipose tissues. The persistent, sterile inflammation characteristic of obesity has been shown to lead to insulin resistance, hyperglycemia, hyperinsulinemia, and steatosis, with downstream diseases such as type 2 diabetes, fatty liver disease, atherosclerosis and various cancers, which increase

in prevalence as adipose tissue mass grows (Zhao et al., 2013, Yang et al., 2010, Hotamisligil 2008).

1.2.1.1 Adipocyte hyperplasia

In normal, non-obese adipose tissue or hyperplastic adipose tissue in obesity, adipocytes demonstrated equilibrium between lipogenic and lipolytic responses. Under these conditions, fat cells have been shown to mobilize or store triglycerides in response to systemic, metabolic demands for energy homeostasis (Guilherme et al., 2008). Dispersal of triglycerides amongst an increased number of cells (hyperplasia) preserves adipocyte function and prevents over-distension of adipocytes, which can lead to inflammation (Weisberg et al., 2003; Jo et al., 2009).

Adipokines, such as leptin and adiponectin, are cytokines secreted by healthy adipocytes. Adipocyte hyperplasia is positively correlated with leptin production which is responsible for maintaining insulin sensitivity and communicating satiety signals to the hypothalamus to decrease food intake or increase energy expenditure (Weisberg et al., 2003; Guilherme et al., 2008; Rosenbaum et al, 1999). Genetic modifications affecting the leptin protein or its receptor lead to hyperphagia, obesity, fertility issues, preferential storage of calories in adipose tissue and many more downstream metabolic issues, displaying the critical role of leptin in maintaining metabolic function and whole-body homeostasis (Rosenbaum et al., 1999). Indeed, the ob/ob knockout mouse model of obesity and metabolic syndrome is the classic phenotypic manifestation of the leptin knockout genotype.

Likewise, adiponectin is responsible for maintaining insulin sensitivity and can serve to decrease triglyceride content in the muscle and liver of obese mice, along with reverse insulin resistance in mice (Yamauchi et al., 2001). Adiponectin expression

correlates with insulin sensitivity, therefore, secretion impairments of this adipokine can result in serious consequences in the glucose metabolism of adipocytes (Yamauchi et al., 2001). Adiposity along with adipocyte hypertrophy lowers adiponectin secretion, which correlates with increased insulin resistance in murine models (Arita et al., 1999; Yamauchi et al., 2001). Overall, both leptin and adiponectin play key roles in maintaining adipose tissue homeostasis, favoring insulin sensitivity and stabilizing nutrient intake.

Alongside the endocrine actions of adipocytes, the adipose stromal cell fraction (ASCF) typically contains resident immune cells such as T regulatory lymphocytes and anti-inflammatory, alternatively activated (M2) macrophages that have been shown to orchestrate secretory functions in adipose tissue. Alternatively activated M2 macrophages along with T regulatory lymphocytes secrete anti-inflammatory cytokines such as IL-10 and TGF- β that protect adipocytes against IL-1 β -, TNF α - and iNOS-mediated inflammatory responses, adipocyte lipolysis, and insulin resistance by suppressing macrophage production of TNF α (Han et al., 2014; Lumeng et al., 2007). M2 macrophages comprise roughly 10-15% of the SCF in traditional adipose tissue depots (Weisberg et al., 2003). In addition to anti-inflammatory cytokines, M2-polarized macrophages produce arginase, which downregulates the pro-inflammatory activity of iNOS (inducible nitric oxide synthase). An endemic anti-inflammatory M2 phenotype contributes to an over-riding immune and inflammatory quiescence in adipose depots. This phenotype has been proposed to sustain normal adipose tissue homeostasis (Lumeng et al., 2007; Shaul et al., 2010; Weisberg et al., 2003).

Endemic T regulatory lymphocytes (Tregs) also have been proposed to contribute substantially, with M2 macrophages, the homeostatic balance in adipose

tissues. Treg lymphocytes augment anti-inflammatory functions contributed by M2 macrophages in adipose depots and directly prevent inflammation by secreting IL-10. In addition, Tregs indirectly blunt inflammatory reactions by promotion of IL-10 secretion from macrophages. Both sources of IL-10 have been determined to maintain insulin sensitivity and adipose inflammatory reactions. In murine models, 10% of the ASCF in non-obese adipose tissue have been determined to be CD3+ lymphocytes (Feuerer et al., 2009). T regulatory lymphocytes comprise 5-20% of the CD4+ subset of CD3+ lymphocytes in most tissues, however, in adipose tissue approximately 50% of the CD4+ cells are Tregs. The data conclusively demonstrated that Treg lymphocytes become selectively sequestered in adipose depots compared to levels observed across other lymphoid and non-lymphoid tissues (Feuerer et al., 2009). The marked increase of Tregs in normal adipose tissue serves to dampen the ongoing Th1 response by conventional T lymphocytes to prevent the synthesis of inflammatory mediators, such as TNF α , which cause insulin resistance (Feuerer et al., 2009). Thus, biased expression of T regulatory lymphocytes in the adipose tissue has been proposed to favor an IL-10-mediated prevention of TNF α -induced insulin resistance in lean or normal adipose tissue (Lumeng et al., 2007; Han et al., 2014).

1.2.1.2 Adipocyte hypertrophy

In response to increases in triglyceride burdens, adipocytes may employ hypertrophic responses (increases in cell size) to accommodate triglyceride excesses during a prolonged nutrient overburdened state (Jo et al., 2009). Shifted balances toward adipocyte hypertrophic responses were determined by homeorhetic (genetic) mechanisms, environmental (diet) influences, and their interactions (Jo et al., 2009; Marti et al., 2008). In these obesity models, nutrient overburdened, hypertrophic

adipose tissue triggered a metabolic inflammatory reaction that ushered in a secondary metabolic syndrome (Weisberg et al., 2003). Limitations on the hypertrophic response of adipocytes to TG storage and overdistended adipocytes from overburdened depots increased secretion of pro-inflammatory adipokines and demonstrated increased levels of cellular apoptosis (Guilherme et al., 2008).

Nutrient-laden, hypertrophic adipocytes secreted higher amounts of pro-inflammatory adipokines TNF α , IL-6, iNOS, and monocyte chemoattractant protein 1 (MCP-1). Monocytes are driven into the adipose tissue in response to MCP-1, which binds the CCR2 receptor to augment monocyte infiltration (Weisberg et al., 2006; Lumeng et al., 2007). MCP-1 and CCR2, knockout approaches clearly demonstrated these chemotactic agents increased monocyte and conventional Th1 T lymphocyte infiltration to the adipose stromal cell fraction (ASCF) (Han et al., 2014; Weisberg et al., 2003). In response to the pro-inflammatory milieu within the ASCF, recruited monocytes are polarized by factors such as LPS and interferon gamma toward differentiation into classically activated (M1), pro-inflammatory macrophage phenotypes (Jo et al., 2009; Lumeng et al., 2007; Shaul et al., 2010; Weisberg et al., 2003). Increased macrophage recruitment into the adipose tissue shifted the composition of the ASCF from 5-10% M2 macrophages in lean animals to upwards of 60% macrophages in obese animals (Guilherme et al., 2008; Weisberg et al., 2003). Newly infiltrated macrophages all differentiated into the M1, pro-inflammatory macrophage and tipped the functional M1/M2 macrophage balance markedly toward the M1 phenotype. Newly recruited M1 phenotypes moreover fused into multinucleated, giant cells that formed crown-like structures around apoptotic, hypertrophic adipocytes (Lumeng et al., 2007). Presumably, these lipid-laden,

multinucleated giant cells served as scavengers of degenerated, apoptotic adipocytes. M1/M2 balances tipped in favor of the M1 phenotype contributed toward a milieu dominated by the inflammatory mediators IL-1 β , TNF α , IL-6, and nitric oxide.

Increased pro-inflammatory cytokine (IL-1 β and TNF α) levels in the ASCF increased inflammatory signal activity in adipocytes, activating MAPKinase (Jager et al., 2010), JNK1 or 2 amino terminal kinase, and NF κ B dependent signal pathways (Zhang et al., 2011, Vallerie et al., 2008). Collectively, these signals phosphorylated serine 307 and 632 on insulin receptors substrate protein 1 (IRS-1), diminished perilipin expression and blocked Glut4 (glucose receptor) expression in adipocytes. The changes are considered molecular hallmarks of inflammation and insulin resistance in nutrient burdened adipose depots and shifted adipocyte metabolic activity towards a lipolytic state. This insulin resistant state in adipose drove release of free fatty acids (FFAs) from the adipocytes, increasing non-esterified fatty acids (NEFAs) levels in circulation (Guilherme et al., 2008; Lumeng et al., 2007). Likewise, TNF α diminished expression of the ligand activated transcription factor, PPAR γ . This transcription factor has been proposed to serve as the co-transactivator of genes whose products drive lipogenesis and preadipocyte hyperplasia, anti-inflammatory macrophage development and Treg T lymphocyte functions in adipose tissues. Diminished PPAR γ levels decreased lipogenesis and increased lipolysis. TNF α -mediated loss of perilipin expression (the protective protein coat around lipid vacuoles in adipocytes) in concert with increased activation of the hormone sensitive lipase (HSL) was shown to drive adipocyte metabolic activity even deeper into a lipolytic state (Guilherme, 2008).

Alongside TNF α -mediated dysregulation of adipocyte function, lipotoxicity and apoptotic adipocytes triggered innate “danger-sensing” Nod-like receptors (NLRs) to activate inflammasome bodies in obese adipose tissue macrophages. Inflammasome activation enables the cleavage of the inactive pro-IL-1 β to the active pro-inflammatory cytokine IL-1 β , which further compounds AT inflammation and the development of insulin resistance (Chawla et al., 2012; Vandanmagsar et al., 2011). These pro-lipolytic alterations in the adipocytes caused by macrophage and hypertrophic adipocyte secretion of TNF α and IL-1 β result in adipose tissue inflammation, insulin resistance, increased lipolysis and increased plasma NEFA levels; all elements seminal to the development of dyslipidemia, steatosis, hyperglycemia, hyperinsulinemia and the onset of metabolic syndrome.

1.2.2 T cell activation and dysregulation in adipose tissue

Apoptotic adipocytes are cleared by tissue macrophages. In association with this scavenger activity, others showed concurrent clonal expansion of T lymphocytes established an adaptive immune response in nutrient burdened adipose depots (Yang et al., 2010). The dominant lymphocyte phenotype belonged to the pro-inflammatory Th1 T lymphocyte subset (Chawla et al., 2012). Both absolute number of T cells (Winer et al., 2009) and proportion of conventional T cells to T regulatory cells (Han et al., 2014) in visceral adipose tissue increased in diet-induced obese mice. Expanded populations of Th1 T lymphocytes expressed high levels of the pro-inflammatory cytokines interferon gamma (IFN γ), lymphotoxin B, and several chemokines that further influenced the pro-inflammatory environment initiated by ATMs.

Not only are there more T-conventional cells in obese adipose tissue undergoing clonal expansion, but the existing T regulatory cells have been shown to

lose their anti-inflammatory lineage and demonstrate a Th1-like phenotype in the presence of excess insulin (Han et al., 2014). Hyperinsulinemia is an event downstream of insulin resistance, caused by an increased secretion of insulin by the β cells of the pancreas from inability of the liver, muscle, and adipose tissue to respond to insulin. Increased concentrations of insulin cause alterations in Treg production of anti-inflammatory cytokine IL-10, along with promote increases in the production of IFN- γ and macrophage production of TNF α , a complete reversal of the traditional role of T regulatory lymphocytes (Han et al., 2014). As adiposity increases, immune dysregulation of both the innate and adaptive immune systems orchestrates upstream adipose tissue inflammation. Adipose inflammation secondarily gives rise to systemic insulin resistance, hyperglycemia, hyperinsulinemia, dyslipidemia, steatohepatitis and the chronic, unresolving, systemic, sterile inflammation characteristic of obesity and metabolic syndrome. The binary signal flow between immune and metabolic systems underpins the pathogenesis of metabolic syndrome associated with adiposity.

1.3 Adiposity in dairy cows

1.3.1 Industry standards to increase adiposity

Universally, dairy industry nutritional programs are designed to deliberately increase adiposity in dairy cattle during end stage lactation by adding 100-150 lbs of weight to cows prior to entering the dry period. Nutritional programs increase fat mass starting in mid lactation, where recommended body condition score is 2.5 or below. Dairy cows are expected to complete a lactation with sufficient increase in adipose tissue mass to achieve a recommended body condition score of 3.0 to 3.5 (Buckley et al., 2003; Mulligan et al., 2006). One numerical shift of body condition

score represents upwards of 100-150 lbs, a considerable increase in adiposity for dairy cows to accumulate during late lactation. This deliberate increase in adipose tissue mass was designed to accommodate heavy energy losses demanded by high amounts of lactation following parturition (Dann et al., 2006; Grummer, 1995).

1.3.2 Shift from lipogenesis to lipolysis at parturition

The peripartal transition from a nonlactating, lipogenic metabolism to the heavy post-partum energy requirements of lactation shifted metabolic balance in adipocytes from lipogenic to highly lipolytic states supportive of milk production (Sumner-Thomson et al., 2011; Zachut et al., 2012). Metabolic adaptations in transition cows (3wks prepartum to 3 wks postpartum) are designed to counteract the energy demands of a high lactational output which exceeds energy intake due to decreased or inadequate dry matter intake (DMI) after parturition (Ingvarsen et al., 2000). The lipolytic state mobilized triglycerides from visceral and subcutaneous adipose tissue depots. Cows with the greatest peripartal loss of adipose depots also showed the greatest amount of insulin resistance in adipose tissues. These animals displayed classical metabolic markers of a systemic metabolic syndrome, insulin resistance, hyperinsulinemia, hyperglycemia, and increased plasma NEFAs (Zachut et al., 2012). These pivotal findings raise a compelling issue. Was the insulin resistance the principal driving element behind the lipolysis and rapid loss in adipose mass or was the negative energy balance associated with heavy lactation the principal element that drove lipolysis and loss of AT mass. The former suggests adipose inflammatory reactions may have underlied high levels of lipolysis in peripartal adipose depots while the latter implies homeostatic mechanisms (leptin, adiponectin, glucagon, insulin) underpinned the lipolytic responses.

1.3.2.1 Blood metabolite elevations

Peripartal mobilization of energy from SAT and VAT has been widely associated with elevated levels of circulating blood non-esterified fatty acids (NEFA). The mobilized NEFAs serve as energy sources during states of severe negative energy balance typically observed in heavily lactating cattle. Tissues such as skeletal muscle begin using lipids, instead of glucose, as a primary energy source after the onset of lactation because peripartal states of insulin resistance repartitioned glucose uptake away from peripheral tissues to conserve it for intramammary production of lactose during heavy lactation (Adewuyi et al., 2005; Khan et al., 2013; Zachut et al., 2013). Much of the NEFA mobilized from adipose depots has been shown to enter hepatocellular metabolic pathways in the liver. Mesenteric adipose depots accommodating inflammatory reactions during nutrient overburdening have been shown to heavily shower the liver with NEFAs (Nov et al., 2013). Pummeling the liver with NEFAs leads to increased FFA uptake and triglyceride storage by the liver along with downstream steatosis and steatohepatosis; two major issues commonly occurring in transition cows (Drackley, 1999; Graugnard et al., 2013).

1.3.3 Liver options for NEFA influx

NEFAs can be oxidized for energy by hepatic mitochondria (healthy), where triglycerides are coupled to apolipoproteins B and E for export as very low-density lipoproteins (VLDLs) for deposition into ectopic adipose depots and synthesis of milk fat (Bernabucci et al., 2004). However, the liver has a limited capacity to convert all NEFAs into triglycerides for export, and therefore may employ alternative pathways to dispose of excess NEFAs. There are three other options the liver can employ for disposal of NEFA influx. When plasma NEFA levels exceed the oxidative capacity of

the mitochondria, the liver begins converting acetyl CoA from fatty acid oxidation into ketone bodies (β HBA) for export to peripheral tissue for energy purposes in a time of glucose reallocation to the mammary gland (Adewuyi et al., 2005, Drackley et al., 2001; Grum et al., 1996). If plasma NEFA concentrations remain high, the liver must resort to peroxisomal β -oxidation (unhealthy oxidation), which can account for a greater fraction of total hepatic oxidation during times of NEFA overload (Grum et al., 1996). When triglycerides are being synthesized faster than they are being exported in the liver, the liver must resort to storage of triglycerides as vacuoles in hepatocytes, leading to loss of hepatocyte function, fatty degeneration of the liver and hepatic lipodosis (Bernabucci et al., 2004, Bobe et al., 2004).

In cases of increased dietary fat intake and obesity in dairy cows, NEFA mobilization may become so great that it exceeds hepatocellular capacity to metabolically cope with heavy influx of NEFA. TG synthesis and storage in hepatocytes has been shown to lead to fatty liver disease and diminished peripartal liver function (Bobe et al., 2004). Fat accumulation in the liver occurs in upwards of 50% of dairy cows in the 4 weeks following parturition (Jorritsma et al., 2000, 2001; Bobe et al., 2004) and is worsened with peripartal obesity. Along with decreasing liver function and disturbed regulation of immune function, fatty liver disease has been shown to erode reproductive efficiency with a 30% reduction in the probability of pregnancy and 35% reduction in probability of estrus in dairy cows (Jorritsma et al., 2000). Steatohepatosis is associated with lower milk yields, reduced fertility and increased cull rates in dairy cows (Bobe et al., 2004). Elevated NEFAs and metabolic insults associated with parturition lead a high percentage of peripartal cattle to develop a metabolic syndrome-like phenotype of insulin resistance (Zachut et al., 2013),

hyperglycemia, hyperinsulinemia, ketonemia, dyslipidemia and fatty degeneration of the liver (Drackley, 1999). These metabolic disturbances in the transition cow mimic seminal events in murine and human models associated with adipose tissue inflammation, immune cell infiltration, metabolic syndrome and type 2 diabetes.

1.3.4 Previous studies of bovine AT inflammation

Recently, Akter et al. (2012) explored the possibility that inflammatory and immune cells could infiltrate bovine adipose depots during increased adiposity. They reported few to no phagocytic immune infiltrates occurred in subcutaneous or visceral adipose tissue depots and concluded little to no inflammatory reaction was associated with nutrient overburdened adipose tissue from over-conditioned dairy and beef cattle (Akter et al., 2012). Akter et al. (2012) utilized immunohistochemistry with bovine macrophage markers designed for flow cytometry, along with a medley of different beef cows, dairy cows, and treatments in the study. The use of insensitive immunologic techniques and the presence of genetic, diet and age confounders likely contributed to the negative results of this study. Nevertheless, the authors concluded inflammatory reactions were not contributing elements in the peripartal metabolic syndromes of heavily conditioned bovines

While their data may be indicative of a protective mechanism for dairy cows in handling increased adiposity, the current study attempts to identify and quantify immune cell infiltrates through use of fluorescence activated cell sorting (FACS) analysis rather than immunohistochemistry, which can often be much less sensitive. We proposed to readdress the issue using a different approach because the data reported by Akter et al. (2012) was inconsistent with mouse and human models of obesity and metabolic inflammatory syndrome.

1.3.5 Importance of research

Adipose tissue inflammation is widely accepted as part of the etiology behind systemic inflammatory phenotypes associated with insulin resistance, dyslipidemia, hepatosteatitis, and the subtle, chronic, unresolving inflammatory disease in models of obesity. Nutritionists and endocrinologists have traditionally attributed these adaptations in metabolism to accommodate heavy lactation and a negative energy balance in periparturient dairy cows, however, adipose tissue physiology has yet to be elucidated. Borrowing upon the body of data in other species, we hypothesize that the industry-wide practice of expanding adipose tissue mass 8-12 weeks prior to calving overloads visceral, omental, and subcutaneous adipose tissue with lipids, with adipocytes storing nutrient excesses in a hypertrophic manner. We propose the hypertrophic adipocyte response to fat storage triggers macrophage and lymphocyte infiltration of visceral adipose tissue depots, which could lead to adipose tissue inflammation in peri-parturient dairy cows. The importance of the research is to determine if nutritional standards to deliberately increase fat mass in dairy cows before parturition are potentiating a metabolic syndrome-like phenotype of chronic, systemic, unresolving, sterile inflammation. If cows present with adipose tissue inflammation, the chronic, sterile inflammation characteristic of obesity could be partly responsible for the sterile inflammatory disease underpinning chronic, nonhealing ulcerative diseases of the bovine foot; one of the largest, unresolved issues in the dairy industry.

1.3.6 Hypothesis and Objectives

The hypothesis of this study is that bovine adipocytes increase in size (hypertrophy) in direct proportion to increased states of adiposity, and that immune and inflammatory cells exist as endogenous inhabitants of these adipose depots.

The objectives of this study are to characterize the relationship of body condition score and adipocyte size in a library of mesenteric, omental and subcutaneous AT depots from lean and heavy lactating dairy cows and to determine immune cell infiltrates within mesenteric adipose tissue stromal cell fraction.

Chapter 2

MATERIALS AND METHODS

2.1 Materials

2.1.1 Reagents

Phosphate buffered saline (PBS) with dextrose, no divalent cations was used to isolate the lymph node crude cell fraction. Hank's Balanced Saline Solution (HBSS) consisting of PBS with divalent cations, dextrose, 10mM HEPES was used to isolate adipose tissue stromal cell fraction. Type II crude collagenase (100mg, 125U/mg) from *Clostridium histolyticum* was obtained from Sigma Aldrich (St. Louis, MO, USA). Heat inactivated (56C, 30min) horse serum was obtained from Sigma Aldrich, (St. Louis, MO, USA) Heat inactivated (56C, 30min) goat serum was obtained from Jackson ImmunoResearch (West Grove, PA, USA). Acid-citrate-dextrose (ACD) consisting of 0.48% (w/v) citric acid, 1.32% (w/v) sodium citrate, 1.47% (w/v) glucose in PBS (no divalent cations, with dextrose) was used to create buffer solutions for antibody staining protocol. First wash buffer consisted of PBS (no divalent cations, with dextrose), 10% acid-citrate-dextrose (ACD) and 2% equine serum. Second wash buffer consisted of PBS (no divalent cations, with dextrose) and 10% acid-citrate-dextrose (ACD). Third wash buffer consisted of PBS (no divalent cations, with dextrose), 10% acid-citrate-dextrose (ACD) and 2% goat serum. Fixation performed using 1% paraformaldehyde in PBS (no divalent cations, with dextrose).

2.1.2 Antibodies

Working stocks of 15 µg/ml (in 0.09% azide) of primary monoclonal antibodies in first wash buffer (PBS 2% ES) kept refrigerated were obtained from Monoclonal Antibody Center, Washington State University (Pullman, WA, USA) (Table 1).

Fluorescein isothiocyanate (FITC)-conjugated AffiniPure goat anti-murine IgG, Fcγ Subclass 1 secondary antibodies, and R-phycoerythrin (PE)-conjugated AffiniPure goat anti-murine IgG Fcγ subclass 2b secondary antibodies were obtained from Jackson ImmunoResearch (West Grove, PA, USA), both used at a 1:100 dilution.

mAb	Isotype	Specificity	2° Ab
MM10A	Murine (IgG2b) anti-bovine	Bovine CD11b on monocyte/macrophage/dendritic cell	Caprine anti-murine PE conjugate
DH59B	Murine (IgG1) anti-bovine	Bovine CD172 on monocyte/macrophage/dendritic cell	Caprine anti-murine FITC conjugate
MM1A	Murine (IgG1) anti-bovine	Bovine CD3 on T lymphocytes	Caprine anti-murine FITC conjugate

Table 1: Monoclonal primary antibodies employed to immunophenotype AT macrophages and lymphocytes in bovine ASCF and lymph node crude cell fraction (Bill Davis, Washington State University School of Veterinary Medicine, Monoclonal Antibody Center, Pullman, WA, USA) and corresponding fluorescent-conjugated secondary antibodies (Jackson ImmunoResearch, West Grove, PA, USA)

2.1.3 Equipment

A refrigerated centrifuge was used for centrifugation of 96-well plate carriers and 50ml conical tubes during tissue isolation and staining procedures. A refrigerated plate vortexer was employed during the staining procedure to loosen cell pellets. Flow cytometric analyses were performed on a FACSCalibur flow cytometer.

2.1.4 Supplies

96-well polystyrene V-bottom plates were obtained from Costar, Sigma Aldrich (St. Louis, MO, USA) for use in staining procedures. Micropipettor tips were obtained from Fisher Scientific (Pittsburgh, PA, USA). Tissue culture flasks (25cm²) were obtained from Corning Incorporated (Corning, NY, USA). Both 15ml and 50ml conical tubes were obtained from BD Falcon (Franklin Lakes, NJ, USA). Tubes (12 x 75 mm) for flow cytometric analysis with a 35µm Cell Strainer Cap were obtained from BD Falcon (Franklin Lakes, NJ, USA).

2.2 Methods

2.2.1 Animal subjects

Lactating, 3-5 year old, multiparous Holstein Friesian cows (n=13) presenting to an abattoir for slaughter or to the George D. Widener Hospital for Large Animals (School of Veterinary Medicine, University of Pennsylvania) for surgical correction of uncomplicated left or right displacement of the abomasum, cesarean section, or cecal torsion were scored for body condition (Table 2). Body condition was scored using a scale of 1 to 5 in increments of 0.25 through visual assessment of the lumbar transverse processes, tuber ischium (pin bones), tuber coxae (hook bones), thurl, tail head, sacral ligament, and ribs according to Penn State Body Condition Scoring-Dairy

Cattle Nutrition (Heinrichs et al., 1989; Roche et al., 2009). Cows with a BCS below 2.5 (Figure 1) were considered lean and cows with a BCS of 3.5 and above (Figure 2) were considered heavy.

Body Condition Score	Description
1	Severely under-conditioned; very thin, emaciated. Tailhead bones easily discernible and deep cavities around tailhead, prominent backbone, lumbar transverse processes clearly visible, hooks/thurl/pins very prominent and sharp with V-angle between hooks and pins, thin legs, poor muscle condition
2	Under-conditioned; thin. Tailhead prominent; somewhat hollow but has modest covering of flesh, limited skin cover, prominent backbone, limited skin cover on lumbar transverse processes (visible $\frac{3}{4}$ of distance), angular hooks/pins with prominent thurl and V-angle between hooks and pins
3	Good body condition. More flesh covering backbone, no deep depressions or fat deposits around tailhead, smooth tips of lumbar transverse processes, hooks and pins rounded, smooth. Soft V-angle between hooks, thurl and pins.
4	Over-conditioned; overweight. Backbone barely visible, lumbar transverse processes very smooth, tips barely visible. Hooks and pins very smooth/rounded but visible, flat, U-angle between hooks and pins. Rump and thurl flat, sacral and tailhead ligaments not visible.
5	Severely over-conditioned; obese. Backbone not visible, lumbar transverse processes flat, bones not visible, hooks/pins not visible/U-angle between hooks and pins, flat over rump and tailhead. All boney prominences from behind rounded and covered in fat, tailhead buried in fat, fat deposits seen on rump and legs.

Table 2: Body condition score scale from 1-5 adapted from Penn State Body Condition Scoring System (Heinrichs et al., 1989, <http://extension.psu.edu/animals/dairy/nutrition/nutrition-and-feeding/body-condition-scoring>, 2004)



Figure 1. Underweight cow, BCS=2.25. Visible hooks and pin bones with a V-shaped thurl. Backbone prominent; can easily see transverse lumbar processes.



Figure 2. Overweight cow, BCS=4.5. Hooks and pins not visible, U-shaped thurl, rounded back, cannot discern transverse lumbar processes.

2.2.2 Adipocyte sizing

Adipose tissue samples (1 cm³) (n=13) were obtained from (1) subcutaneous adipose tissue (SAT) depot caudolateral to the rectus abdominus muscle (2) omental adipose tissue from the superficial leaf of the greater omentum, and (3) mesenteric adipose tissue located in the mid-jejunum. Samples were excised using single-edged surgical carbon-steel blades during surgery or immediately after slaughter, then cut to 1 cubic centimeter with Metsenbaum scissors to allow complete immersion in fixative. Samples were incubated (24h, 25C) in 10% buffered formalin, embedded in paraffin, sectioned (5 µm), mounted on glass slides, and stained with hematoxylin and eosin.

Adipocyte cross-sectional area was determined for 100 randomly selected adipocytes from each adipose tissue depot via measurement of 20 randomly selected adipocytes from 5 randomly selected fields (100X) using Nikon Imaging System Elements D image analysis software (Nikon DS-FI2 Camera, Nikon Instruments Inc., Japan) (Figure 3).

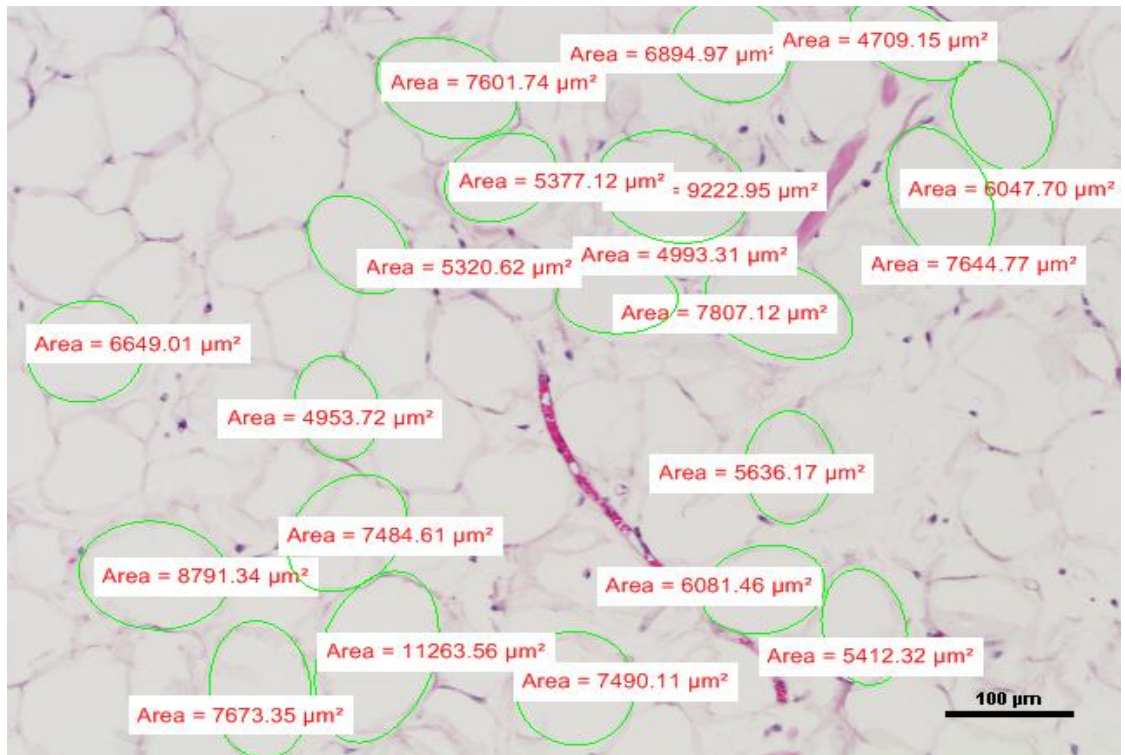


Figure 3. Mesenteric adipocyte cross-sectional area (μm) of 20 randomly selected adipocytes from a randomly selected field (100X).

2.2.3 Lymph node crude cell fraction isolation

Mid-jejunum mesenteric lymph nodes were removed (n=7) using surgical carbon-steel blades and placed in PBS (4C) for crude cell fraction isolation to serve as

a positive control. Excised lymph nodes in PBS were cut longitudinally and the crude cell fraction from the medulla and cortex (without the capsule) was scraped from the node (4C). Lymphoid tissue was passed through a glass wool column and washed with PBS to collect cell eluent from column. Cell eluents were washed with PBS (3X, 1200rpm, 20 min, 4C) and resuspended in first wash buffer (4C, 1.0×10^7 cells/ml).

2.2.4 Adipose tissue SCF isolation

2.2.4.1 Collagenase preparation

Type II collagenase was suspended (10mg/ml) in PBS (with dextrose, no divalent cations) with stirring (30 min, 25C). Solution was centrifuged (1200rpm, 25C, 20 min) and the supernatant was aliquoted and stored at -20C.

2.2.4.2 Adipose tissue SCF isolation

Mid-jejenum mesenteric adipose tissue samples were excised (n=3) using surgical carbon-steel blades and placed in HBSS, 10mM HEPES, with divalent cations (38C) for stromal cell fraction isolation. Excised adipose tissues were minced (1mmx1mm) in HBSS, 10mM HEPES (38C) and washed once (800rpm, 5min, 25C) to remove vascular components (RBCs, leukocytes) from tissue. Five (1g wet weight) samples per subject were digested individually in tissue culture flasks with Type II collagenase (2mg/ml) in HBSS (10mM HEPES, with divalent cations) and incubated with shaking (150 rpm, 60min, 38C). A magnetic stir bar was added to each flask and the mixtures were stirred for 15 min (38C) to complete digestion of the tissue. Collagenase-digested adipose tissue samples were passed through a glass wool column and washed with PBS, 10mM HEPES (38C) to collect cell eluents. Cell suspensions

were combined, washed (PBS, 10mM HEPES (1X, 1200rpm, 20 min, 25C)) and resuspended in first wash buffer (4C, 1.0×10^7 cells/ml).

2.2.5 Staining for flow cytometry

Lymph node and ASCF cell suspensions in the first wash buffer (1.0×10^6 cells, 4C) were placed, separately, into wells of a 96 well v-bottomed plate (1 million cells/well) on ice for staining with primary monoclonal antibodies (Table 1) as follows: (1) control cells with no primary or secondary antibodies, (2) control cells with FITC (green) and PE (red) fluorescent-conjugated secondary antibodies only; (3) CD11b (macrophages, monocytes/dendritic cells) (4) CD172 (macrophages) (5) CD3 (lymphocytes) (6) CD11b and CD172 (macrophages), and (7) CD11b and CD3 (lymphocytes and macrophages/dendritic cells). Primary mAb cocktails described above were added to the appropriate wells containing ASCF or lymph node crude cell fraction (1.0×10^6 cells) at equal concentrations (15 $\mu\text{g/ml}$), vortexed (30s, 1000g, 4C), and incubated (30 min, 4C).

After incubation, the plate was centrifuged (5 min, 2500g, 4C). Supernatant was removed by flicking the plate and cells were resuspended in a plate vortexer (30sec, 1000g, 4C). Cells were washed (3X) with first wash buffer (4C). After the last wash, appropriate secondary FITC- or PE-conjugated secondary antibodies (1:100 dilution) were added to wells as follows: (1) none, (2) FITC and PE, (3) PE only, (4) FITC only, (5) FITC only, (6) FITC and PE, (7) FITC and PE (Table 1). Secondary Ab cocktails (1:100 dilution) described above were added to the appropriate wells at equal concentrations, vortexed (30s, 1000g, 4C), and incubated (30 min, 4C).

After incubation, plate was centrifuged (5 min, 2500g, 4C), and cells were washed (2X) using second wash buffer. After the last wash, cells were incubated in

1% PBS buffered paraformaldehyde (15 min, 4C), the plate was centrifuged (5 min, 2500g, 4C), the supernatant removed, and the cells resuspended in the plate vortexer (30s, 1000g, 4C). Cells were resuspended in first wash buffer (4C), transfer pipetted through 12 x 75 mm Tube with 35µm Cell Strainer Cap and refrigerated (4C) in preparation for FACS analysis on a FACSCalibur flow cytometer. Staining procedures adapted from Dr. Bill Davis, Washington State University School of Veterinary Medicine, Monoclonal Antibody Center, Pullman, WA, personal communication.

2.2.6 Fluorescence Activated Cell Sorting (FACS) analysis

FACS analysis was performed on a BD (Becton Dickinson) FACSCalibur flow cytometer (CTCR core facility, 007 Wolf Hall; www2.udel.edu/ctcr/ctcr-core-facility). Flow cytometry was performed by analyzing cells traveling through a tube in single file with a laser beam exciting the fluorochrome (FITC or PE) labeled secondary antibody reacting with the primary antibody marker. Emitted fluorescence level is measured for each cell and the flow cytometer gives a population profile of fluorescent staining, displaying which cells express the fluorochrome label and which do not. This fluorescence profile serves to quantify which markers are present on the cells being analyzed within the gated population, expressed as percentage of cells gated in the upper left (UL), upper right (UR) and lower right (LR) quadrants.

FACS analysis was performed to determine (1) percent macrophages/monocytes/dendritic cells (CD11b+), (2) percent macrophages (CD172+), and (3) percent T lymphocytes (CD3+) of both the adipose stromal cell fraction and LN crude cell fraction from a minimum of 10,000 reads per cell fraction. The percentage of total cell fractions was determined from the percentage of gated

events in the three positive quadrants (UL, UR, LR). Gates were established on control cells stained with secondary antibodies only (no primary antibodies) to control for non-specific secondary antibody conjugate binding and gate on a double negative stained population of cells. Gates were deliberately positioned to have at least 97% of negatively stained cells within the lower left quadrant, with 1% of cells in each of the upper left, upper right, and lower right quadrants. Verification of the gating was performed by examining unstained cells which also fell within the double negative (lower left) gate.

Being the FITC (green) and PE (red) conjugates have emission spectra of $530\pm 30\text{nm}$ and $585\pm 40\text{nm}$, respectively, the spectral overlap can cause the fluorescence emission of the FITC fluorochrome to be detected in the PE fluorochrome detector, and vice versa ("Flow," 2012). Compensation was adjusted using single color stained cells to assure proper analysis of multicolor samples through adjusting the portion of one fluorescence detector's signal (FL-2) from the second detector's signal (FL-1), leaving only the desired color signal to eliminate spectral overlap ("Compensation," 2003). Compensation adjustments were performed visually using continuous single-color cell analysis until cells were evenly distributed across the FITC or PE opposing channels for all three sets of single-stained cell controls (Figure 4).

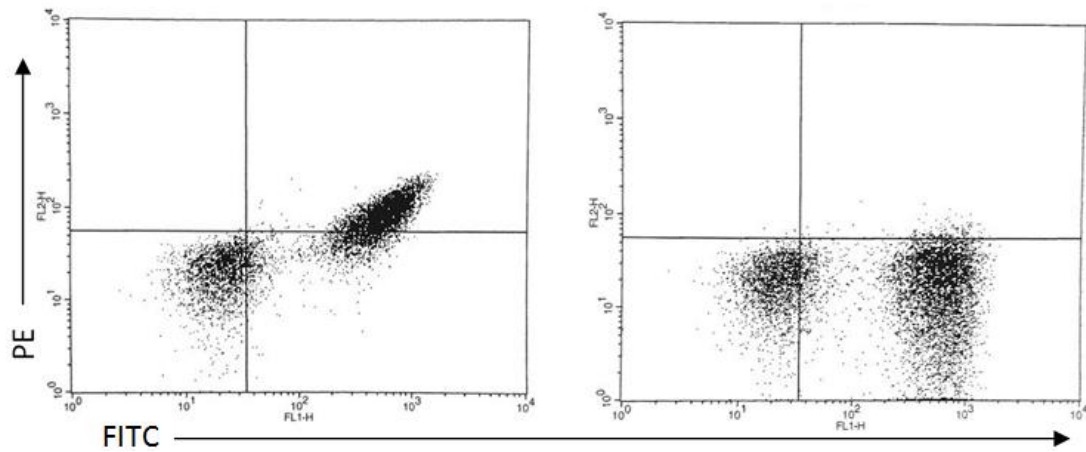


Figure 4. Demonstration of adjustment of compensation for a single color FITC (FL-1) stained set of lymph node cells (stained for CD3). The left picture demonstrates an undercompensated set of cells without enough fluorescence subtraction. The PE median fluorescence intensity of the positive FITC population is greater than that of the negative FITC population. The figure on the right shows proper compensation where the median of the positive and negative FITC population is equal within the PE channel (“Technical Bulletin,” 2009).

Chapter 3

RESULTS

Adipocyte area and frequency distribution of adipocyte size increases with increasing body condition

3.1 Adipocyte area and BCS

To study the relationship between adipocyte size and adiposity, mid-jejunal mesenteric adipose tissue samples were collected from multiparous, lactating Holstein Friesian dairy cows (n=16) and body condition score, a measure of adiposity, was recorded. Increasing adiposity increased mean adipocyte cross-sectional area in mesenteric (Figure 5), omental (Figure 6), and subcutaneous (Figure 7) adipose tissue. The level of adiposity was directly related to mean adipocyte area for the mesenteric (r=0.85), omental (r=0.87), and the subcutaneous (r=0.59) adipose depots.

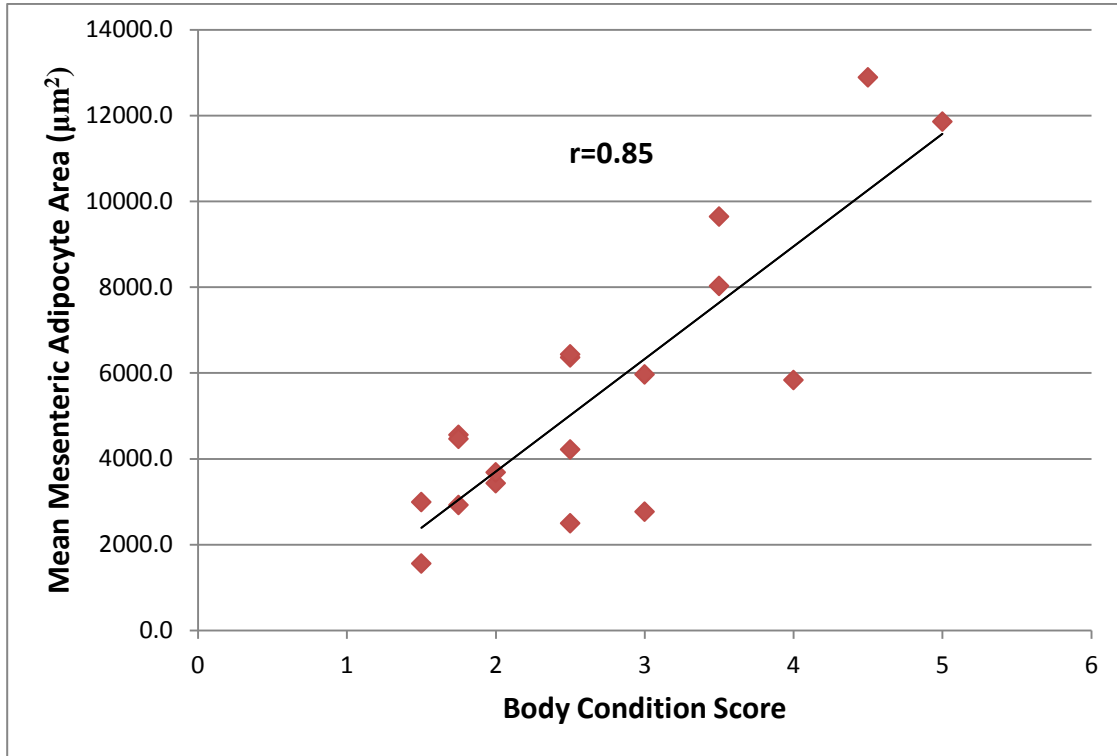


Figure 5. Level of adiposity (body condition) is directly correlated to mean mesenteric cross-sectional adipocyte area (μm^2) in bovine mid-jejunum mesenteric adipose tissue ($r=0.85$) ($n=16$).

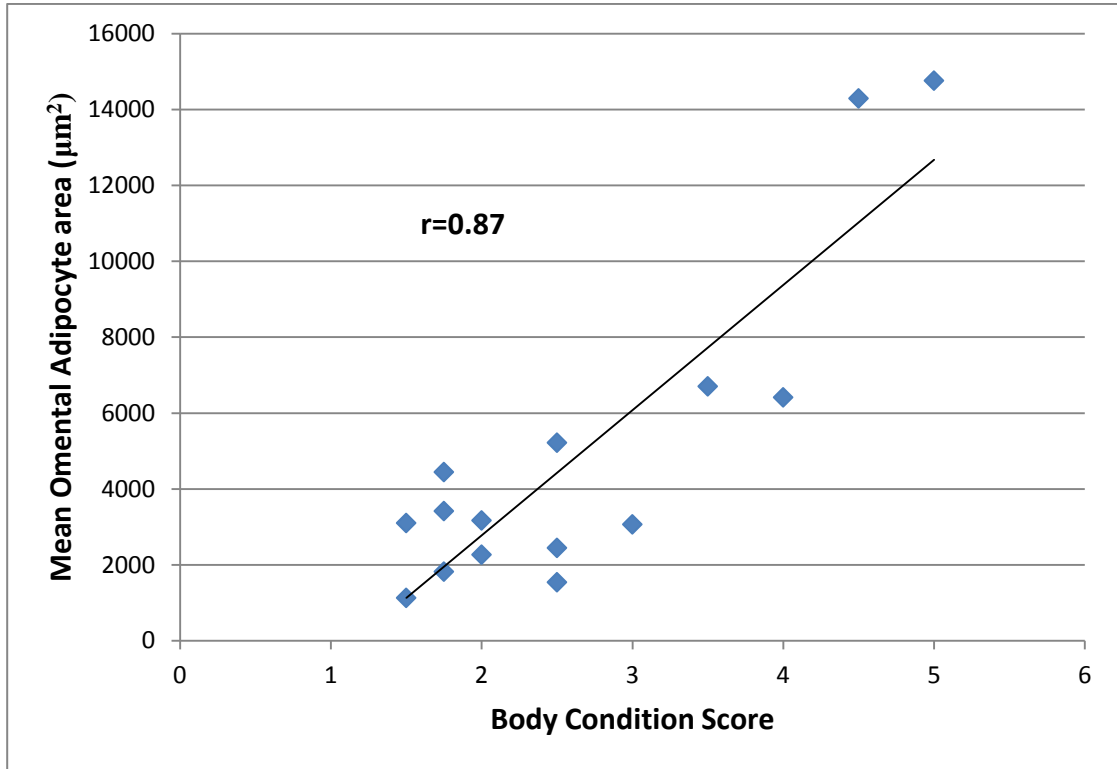


Figure 6. Level of adiposity (body condition) is directly correlated to mean omental cross-sectional adipocyte area (μm^2) in bovine omental adipose tissue ($r=0.87$) ($n=15$).

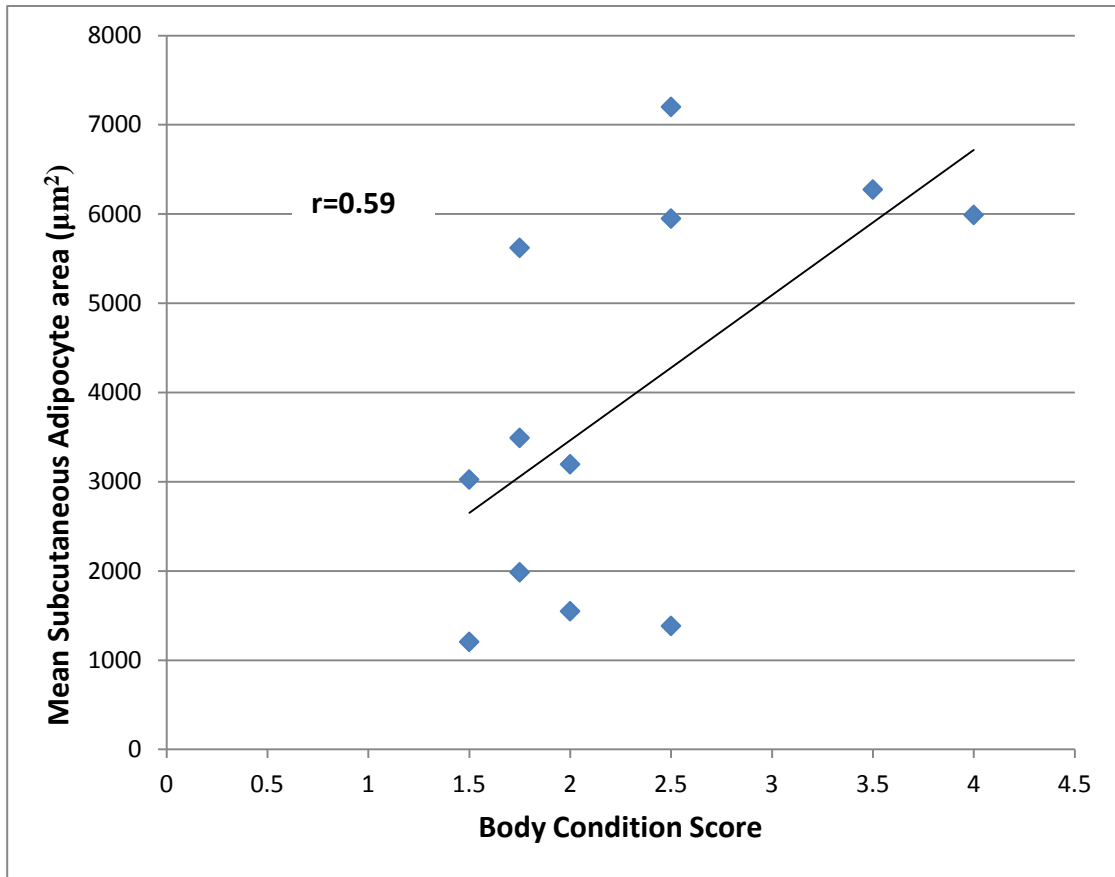


Figure 7. Level of adiposity (body condition) is weakly correlated to mean subcutaneous cross-sectional adipocyte area (μm^2) in bovine subcutaneous adipose tissue ($r=0.59$) ($n=12$).

3.2 Adipocyte size across tissue depots

Mesenteric and omental adipocyte area (μm^2) were directly correlated ($r=0.92$) across all cows, in that mean mesenteric and omental adipocyte sizes increased proportionally (Figure 8). Likewise, mesenteric and subcutaneous adipocyte area (μm^2) were correlated ($r=0.89$), in that mean mesenteric and subcutaneous adipocyte size increased proportionally across all cows (Figure 9). Lastly, omental and subcutaneous adipocyte area (μm^2) were correlated ($r=0.92$), in that mean omental and

subcutaneous adipocyte size increased proportionally across all cows (Figure 10). The data showed adipocyte area increased proportionally across two visceral and one subcutaneous adipose depot in dairy cows.

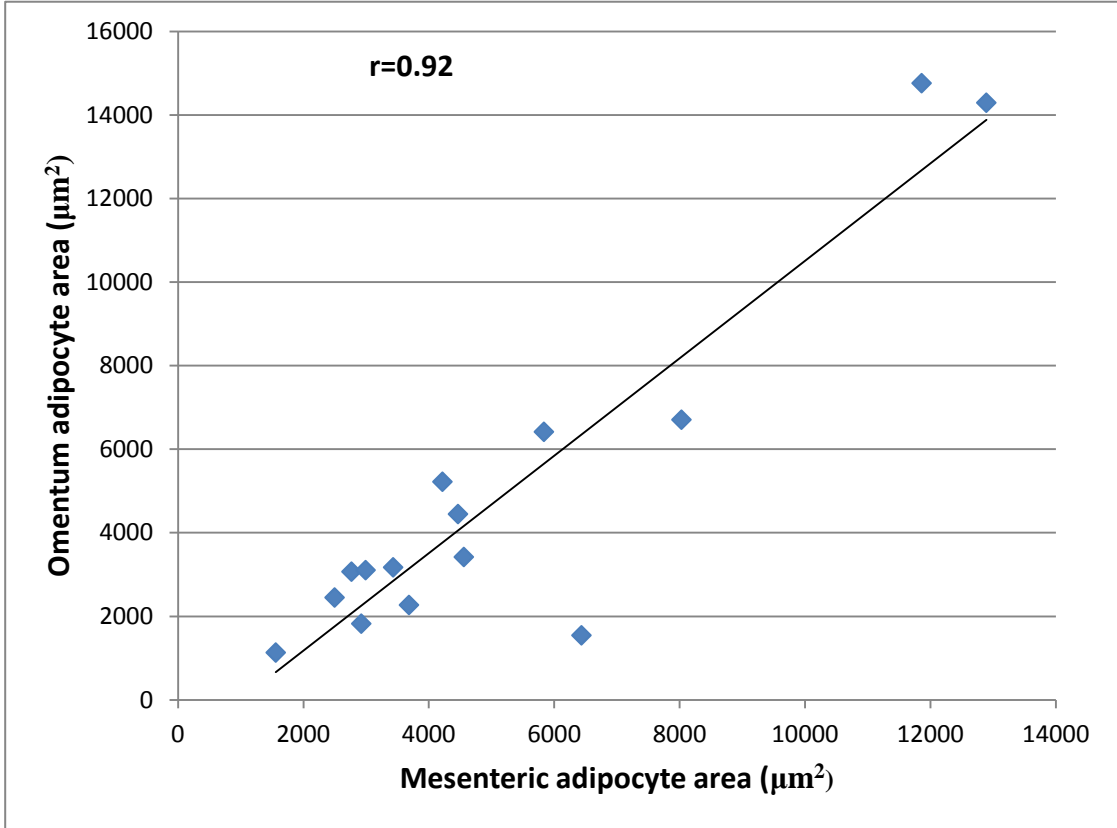


Figure 8. Mean mesenteric adipocyte area (μm^2) was directly correlated ($r=0.92$) with mean omental adipocyte area (μm^2) ($n=15$).

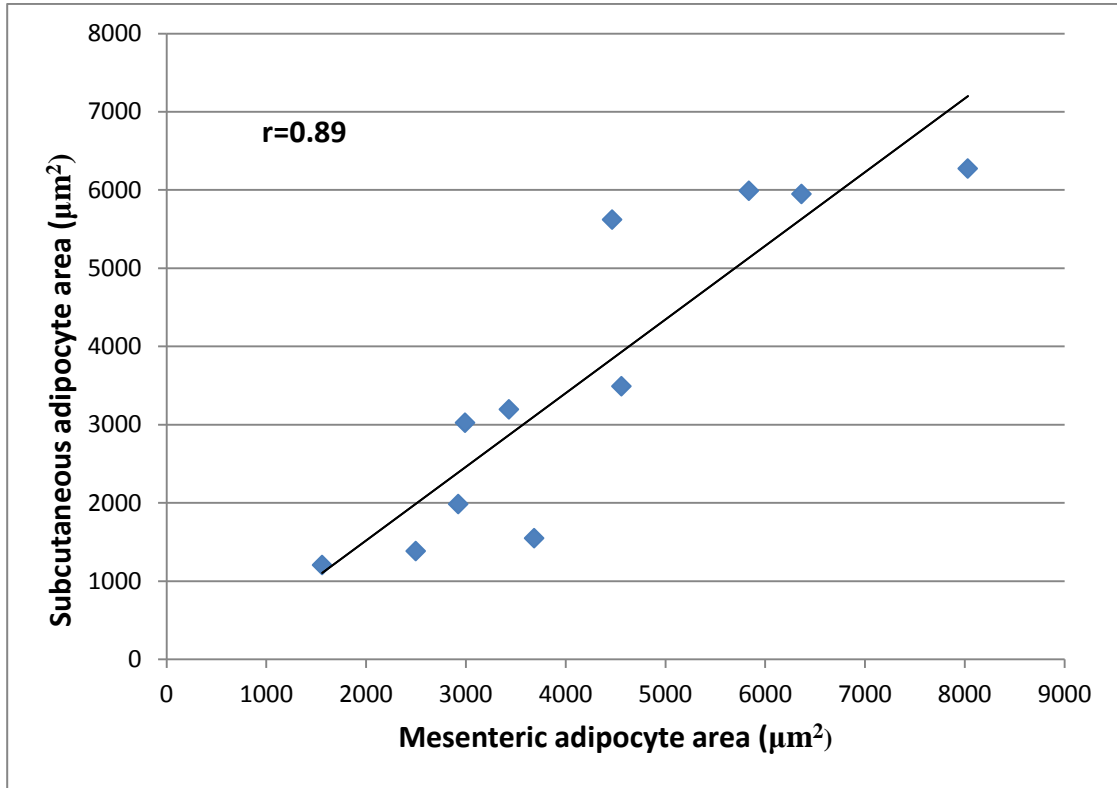


Figure 9. Mean mesenteric adipocyte area (μm^2) was directly correlated ($r=0.89$) with mean subcutaneous adipocyte area (μm^2) ($n=11$).

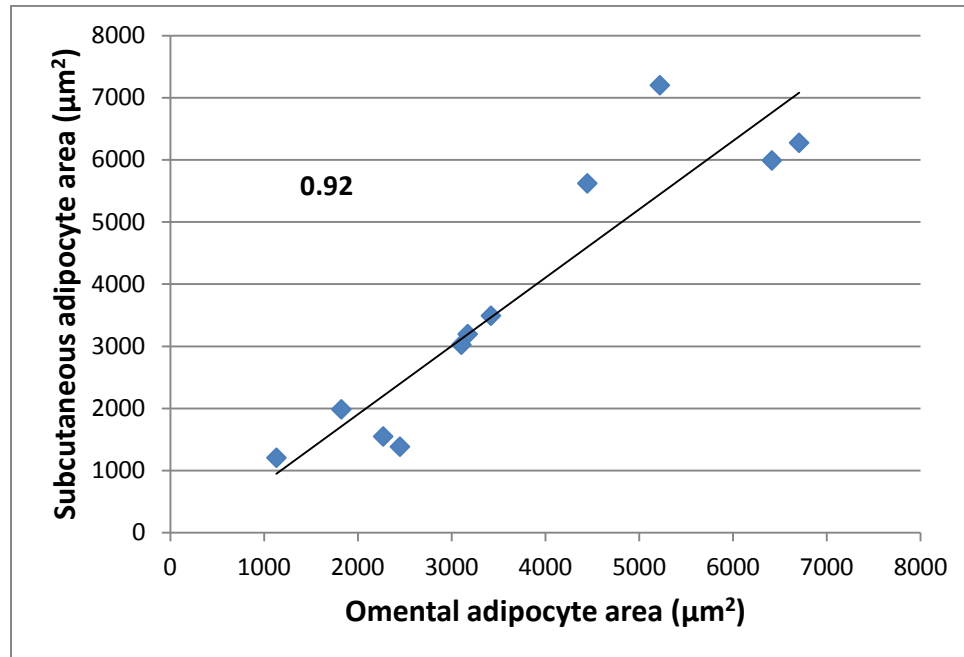


Figure 10. Mean omental adipocyte area (μm^2) was directly correlated ($r=0.92$) with mean subcutaneous adipocyte area (μm^2) ($n=11$).

3.3 Frequency distribution of adipocyte area

The $1000\mu\text{m}^2$ increments in adipocyte size were plotted against the frequency of adipocyte size occurrence within each interval for each level of body condition score within each adipose depots. Increased adiposity was associated with a shift in the entire frequency distribution of adipocyte size toward larger cell sizes in the mesenteric (Figure 11), the omental (Figure 12) and the subcutaneous adipose depots (Figure 13). The results showed the frequency of adipocytes with larger adipocyte area increased while the frequency of adipocytes with smaller adipocyte area decreased when body adiposity (body condition score) increased from lean cows (BCS 1.5, 2.5) to heavy cows (BCS 3.5).

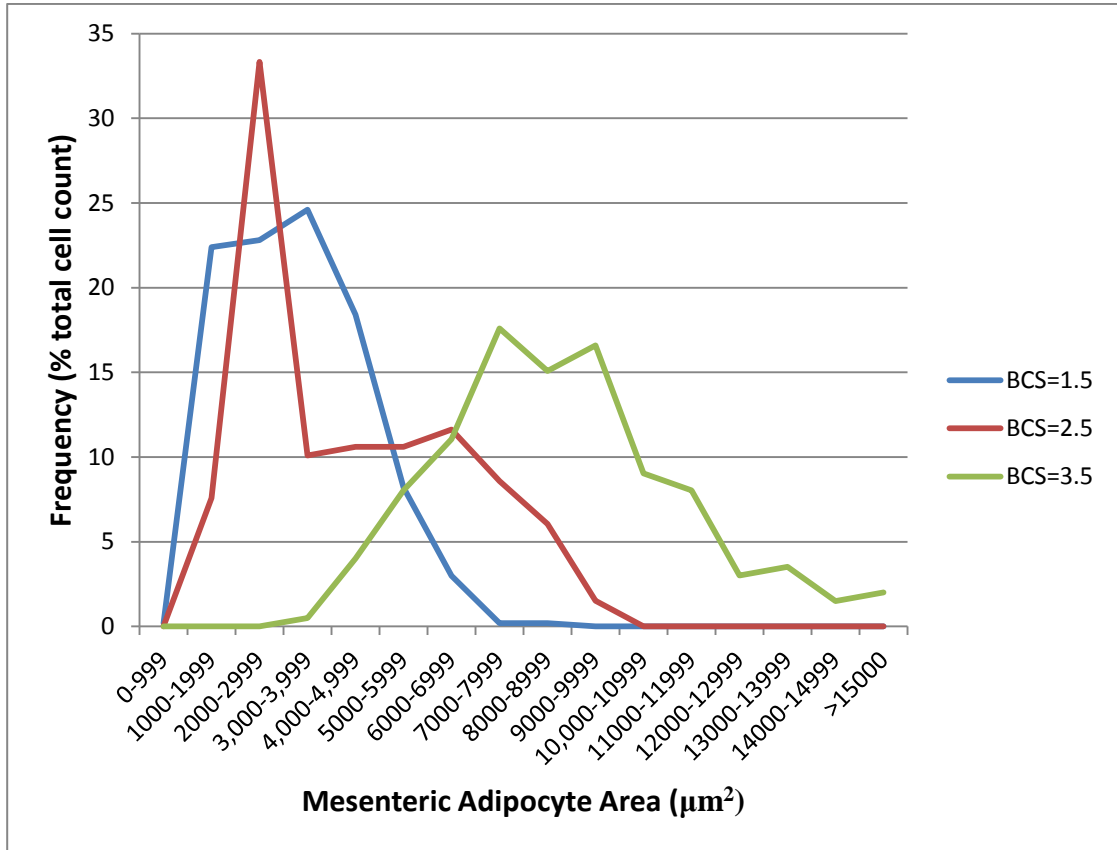


Figure 11. Increased level of adiposity (body condition) shifts the frequency of mesenteric adipocyte cross-sectional area (μm) toward larger cell sizes in lean (BCS 1.5 (n=5), 2.5 (n=2)) and heavy (BCS 3.5 (n=2)) dairy cows.

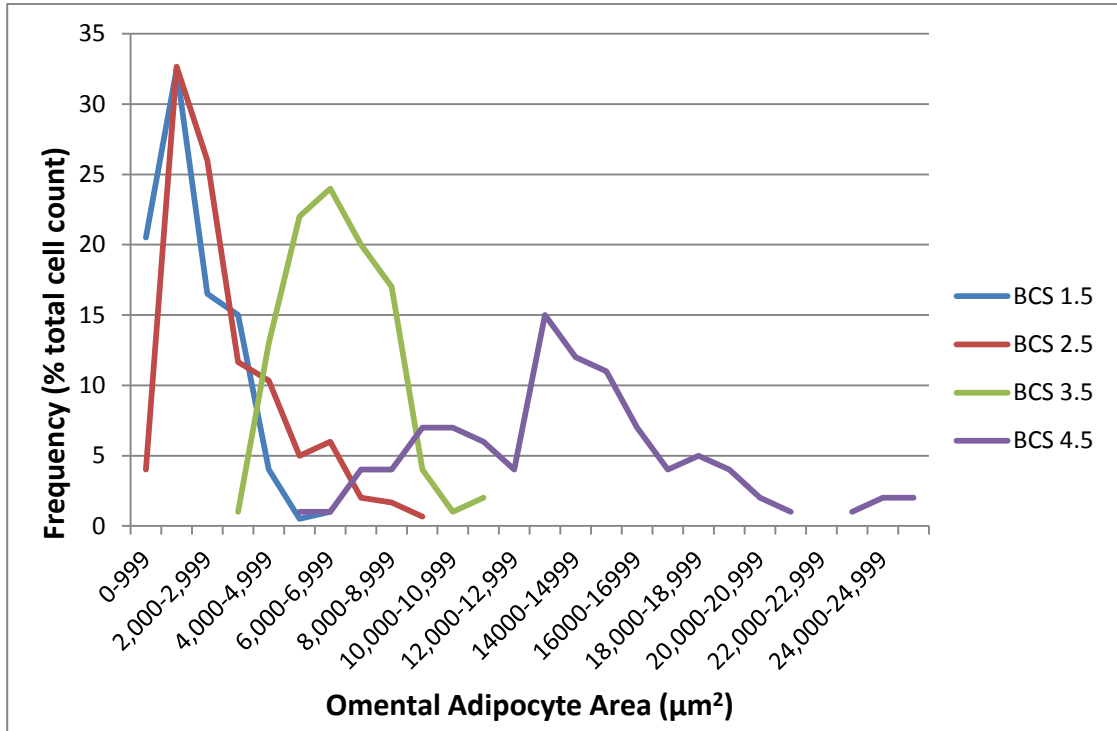


Figure 12. Increased level of adiposity (body condition) shifts the frequency of omental adipocyte cross-sectional area (μm^2) toward larger cell sizes in lean (BCS 1.5 (n=2), 2.5 (n=3)) and heavy (BCS 3.5 (n=1), 4.5 (n=1)) dairy cows.

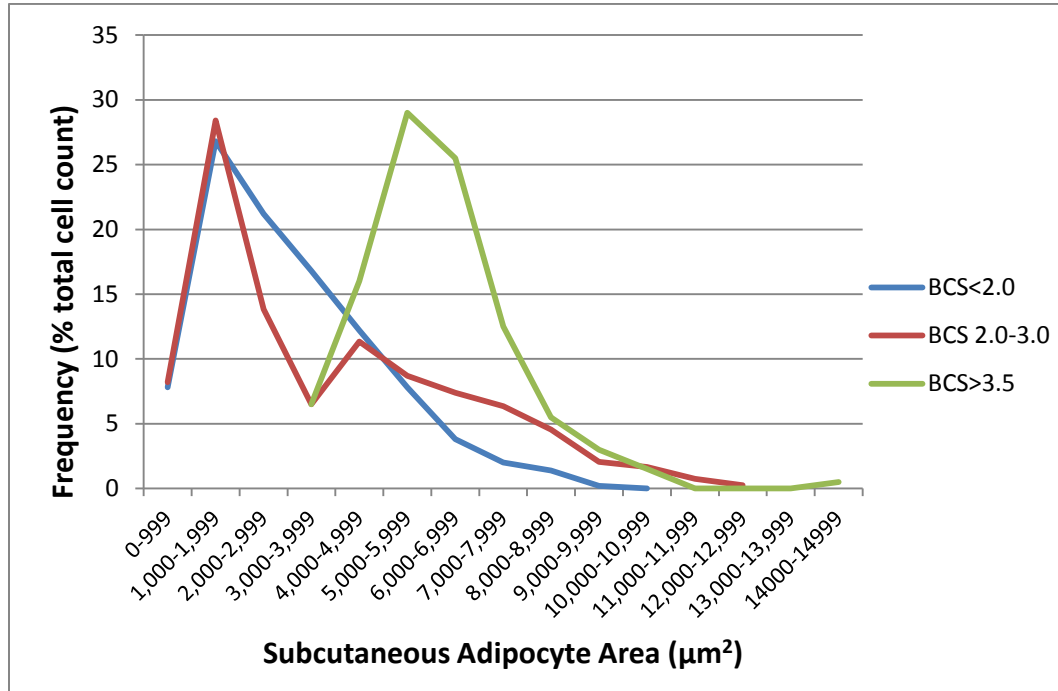


Figure 13. Increased level of adiposity (body condition) shifts the frequency of subcutaneous adipocyte cross-sectional area (μm^2) toward larger cell sizes in lean (BCS <2.0 (n=5), 2.0-3.0 (n=5)) and heavy (BCS >3.5 (n=2)) dairy cows.

T lymphocytes and macrophages are endogenous cell populations in mesenteric adipose SCF

3.4 Immune cell infiltrates in mesenteric adipose tissue

3.4.1 LN population characteristics

A representative cytogram with forward (FSC) and side light scatter (SSC) of a fixed mesenteric lymph node crude cell fraction demonstrated the location of the gated lymph node cell populations (Figure 14). There was little diversity in cell size (FSC) or complexity (SSC), as seen by the small, compact single cell population on the

cytogram. Cells with low forward scatter and varying side scatter along the vertical SSC axis were regarded as dead cells or cellular debris, and were not gated upon to ensure visualization of solely viable, intact cells. The crude cell fraction was gated to exclude only cells which did not fall within the highest density area of cells, keeping the majority of the crude cell fraction within the gate.

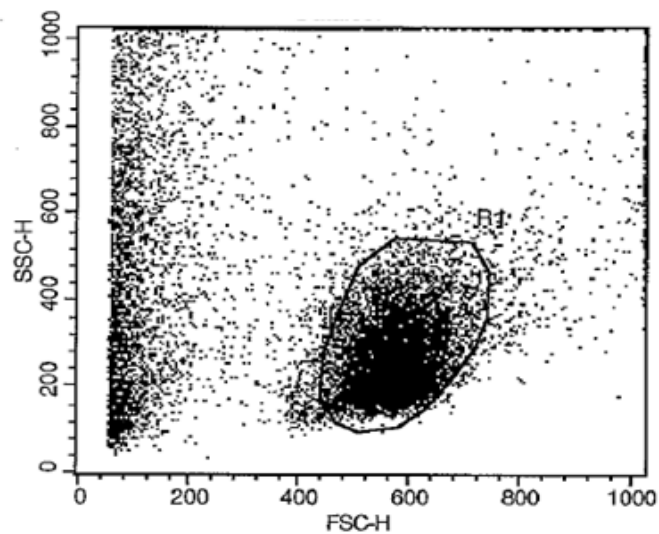


Figure 14. Cytogram of lymph node crude cell fraction cells circled within the gate labeled “R1”. Forward scatter (FSC) and side scatter (SSC) of light from cells were measured by a FACSCalibur flow cytometer and gated cells were analyzed for fluorescence.

3.4.2 ASCF population characteristics

A cytogram with forward (FSC) and side light scatter (SSC) of fixed mesenteric ASCF shows a representative location of the single population of stromal cells (Figure 15). The population displayed a wide diversity in cell size (FSC) and complexity (SSC), and was conservatively gated on the area of highest density cells to

exclude the cells along the periphery of the gate. The gating corresponded with the location of the crude cell population in the lymph node (Figure 14), using the location of macrophages and lymphocytes in the lymph node to determine presence or absence of macrophages and/or lymphocytes in the ASCF. Cells with low forward scatter and varying side scatter along the vertical SSC axis were regarded as dead cells or cellular debris, and were not gated upon to ensure visualization of solely viable, intact cells.

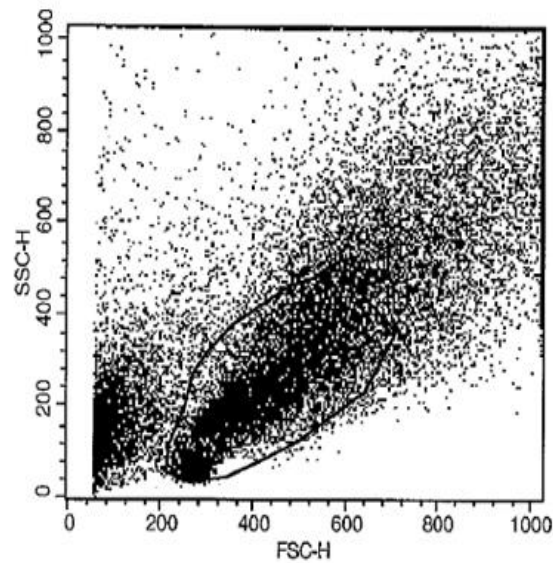


Figure 15. Cytogram of the mesenteric adipose stromal cell fraction circled within the gate. Forward scatter (FSC) and side scatter (SSC) of light from cells were measured by a FACSCalibur flow cytometer and gated cells were analyzed for fluorescence.

3.4.3 Gating controls

Lymph node and ASCF cell auto-fluorescence were accounted for through gating control cells stained with no primary antibodies but double stained with FITC and PE conjugated secondary antibodies. Gating ensured 97% or more of the total cell

fraction fell within the lower left, double negative quadrant in both the lymph node crude cell fraction and the ASCF (Figure 16). Gates were set deliberately to allow approximately 1% of gated events to fall in the UL, UR, and LR quadrants to delineate where cells started expressing fluorescent labels versus autofluorescence of cells (Figure 17). Gating parameters were verified through analysis of unstained control LN and ASCF cells (Figure 18).

A (LN)

B (ASCF)

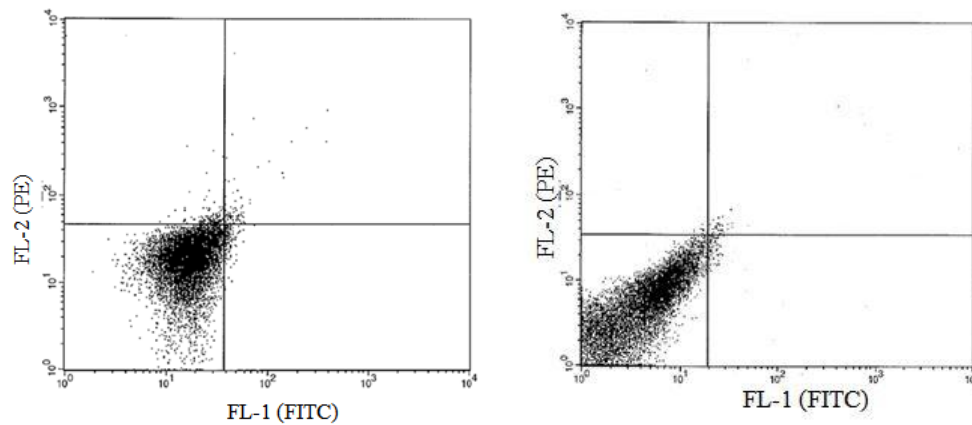


Figure 16 Representative sample of double negative control lymph node crude fraction (A) and adipose stromal cell fraction (B) cells stained with both FITC and PE conjugated secondary antibodies, no primary antibody stain. Quadrant gates were established through analyzing secondary only stain after adjusting for single color stain compensation levels.

Quadrant Statistics

File: Data.002
Sample ID: LN cells secs only
Tube:
Acquisition Date: 10-Apr-14
Gated Events: 10939
X Parameter: FL1-H (Log)
Quad Location: 25, 55

Log Data Units: Linear Values
Patient ID:
Panel:
Gate: G1
Total Events: 14324
Y Parameter: FL2-H (Log)

Quad	Events	% Gated	% Total	X Mean	X Geo Mean	Y Mean	Y Geo Mean
UL	117	1.07	0.82	13.88	11.42	441.01	125.89
UR	47	0.43	0.33	82.44	50.43	161.45	108.47
LL	10654	97.39	74.38	10.25	9.16	17.91	14.68
LR	121	1.11	0.84	30.08	29.37	31.86	28.12

Figure 17. Representative quadrant statistics for control cells stained with secondary antibodies only. Red circles highlight the intentional 1% of cell events falling in the UL and LR quadrants with over 97% of gated events in the LL quadrant.

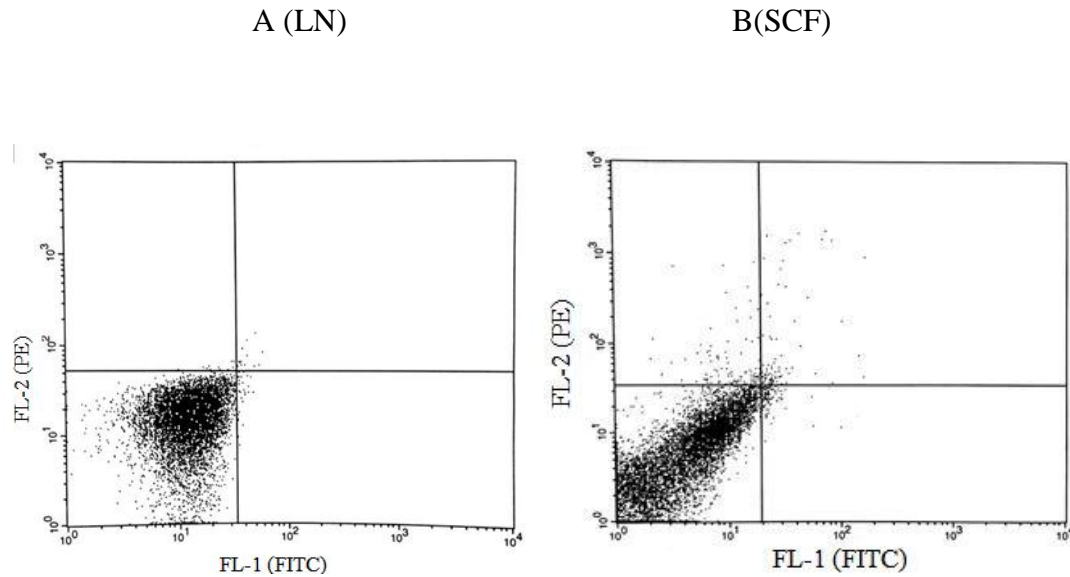


Figure 18. Representative sample of unstained LN crude cell fraction (A) and unstained ASCF (B) for verification of gates set from cells stained only secondary antibodies.

3.4.4 CD11b

The β_2 integrin α -chain CD11b cell surface marker is present on monocytes, macrophages, dendritic cells, and CD8+ effector T lymphocytes and mediates adhesion to endothelial cells and extravasation (Fiorentini et al., 2001). Mesenteric LN cells (n=6) stained with a primary mAb against CD11b and corresponding PE conjugated secondary antibody contained 24.9% \pm 2.47 (mean \pm SEM) CD11b+ macrophages/dendritic cells/CD8+ T cells (Figure 19, A). Mesenteric ASCF cells (n=3) stained with a primary mAb against CD11b and corresponding PE conjugated secondary antibody contained 12.7% \pm 4.3 CD11b+ macrophages/dendritic cells/CD8+ T cells (Figure 19, B).

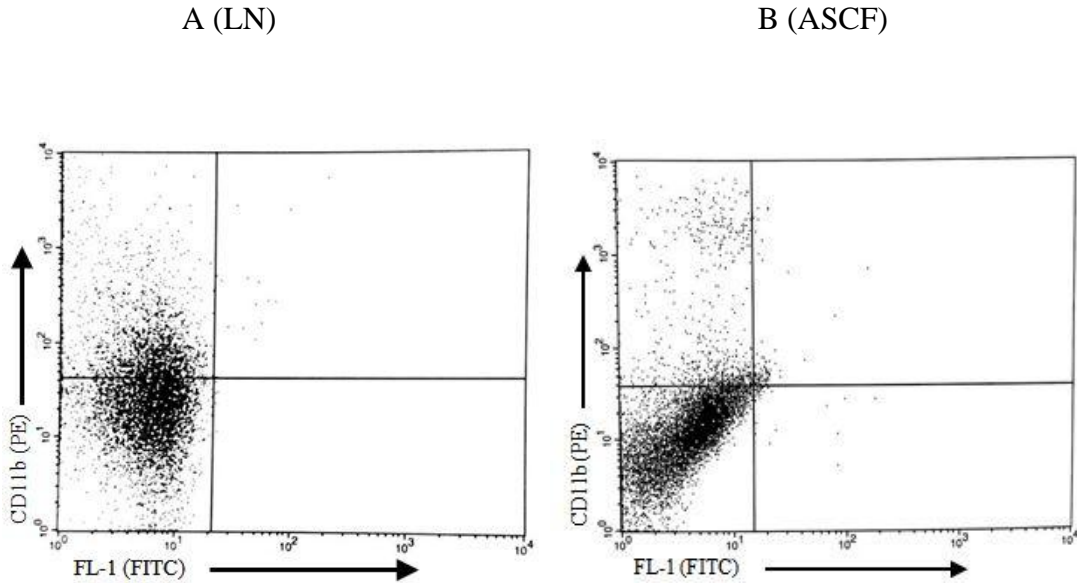


Figure 19. Representative sample of CD11b⁺ macrophages, dendritic cells, and CD8⁺ effector T lymphocytes comprise 24.9%±2.47 (mean±SEM) (n=6) of the LN crude cell fraction (A) and 12.7%±4.3 (n=3) of the ASCF (B) as seen in cells positively emitting PE fluorescence in the UL quadrants.

3.4.5 CD172

CD172, also known as SIRP α (signaling regulatory protein α) or macrophage fusion receptor, binds CD47 and is a transmembrane regulatory protein expressed by myeloid cells (macrophages, monocytes, dendritic cells) and is essential for multinucleate giant cell formation and leukocyte trafficking (Waters et al., 2009). Mesenteric LN cells (n=6) stained with a primary mAb against CD172 and corresponding FITC conjugated secondary antibody contained 6.4%±0.9 (mean±SEM) CD172⁺ macrophages/dendritic cells/monocytes (Figure 20, A). Mesenteric ASCF cells (n=3) stained with a primary mAb against CD172 and corresponding FITC conjugated secondary antibody contained 14.8%±8.7 CD172⁺ macrophages/dendritic cells/monocytes (Figure 20, B).

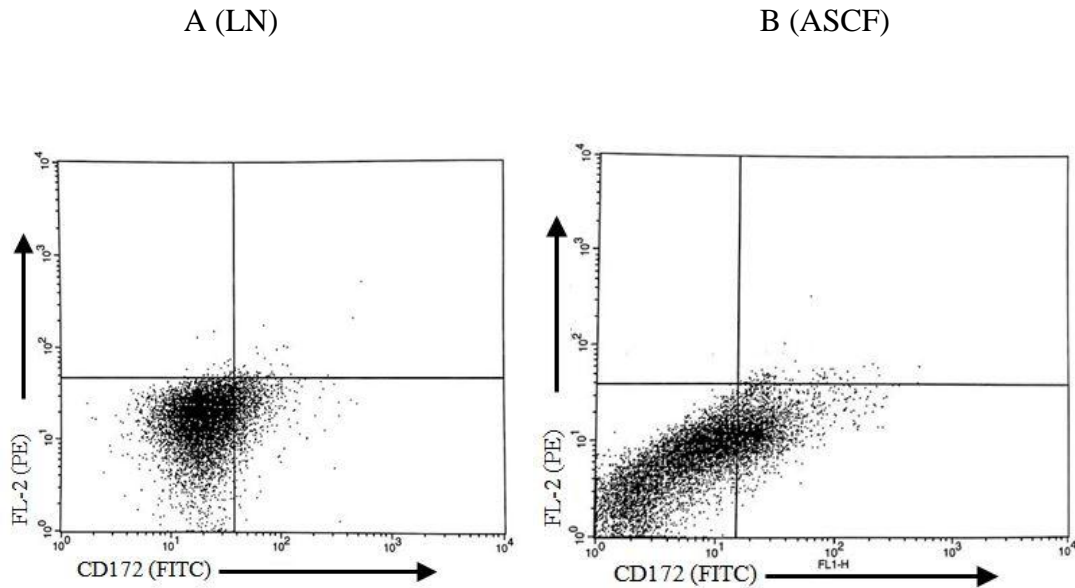


Figure 20. Representative sample of CD172+ macrophages, dendritic cells, and monocytes comprise $6.4\% \pm 0.9$ (mean \pm SEM) ($n=6$) of the LN crude cell fraction (A) and $14.8\% \pm 8.7$ ($n=3$) of the ASCF (B) as seen in cells positively emitting FITC fluorescence in the LR quadrants.

3.4.6 CD3

Cell surface protein CD3 is expressed on bovine $\alpha\beta$ and $\gamma\delta$ T cells in the T cell receptor (TCR) complex, expressed specifically on T lymphocytes. On the cell surface, the TCR is a heterodimeric molecule with paired $\alpha\beta$ or $\gamma\delta$ chains expressed in a complex with CD3, which is responsible for signal transduction critical for T cell activation (MacHugh et al., 1998). Mesenteric LN cells ($n=6$) stained with a primary mAb against CD3 and corresponding FITC conjugated secondary antibody contained $77.9\% \pm 3.5$ (mean \pm SEM) CD3+ T lymphocytes (Figure 21, A). Mesenteric ASCF cells ($n=3$) stained with a primary mAb against CD3 and corresponding FITC conjugated secondary antibody contained $7.9\% \pm 1.1$ CD3+ T lymphocytes (Figure 21, B).

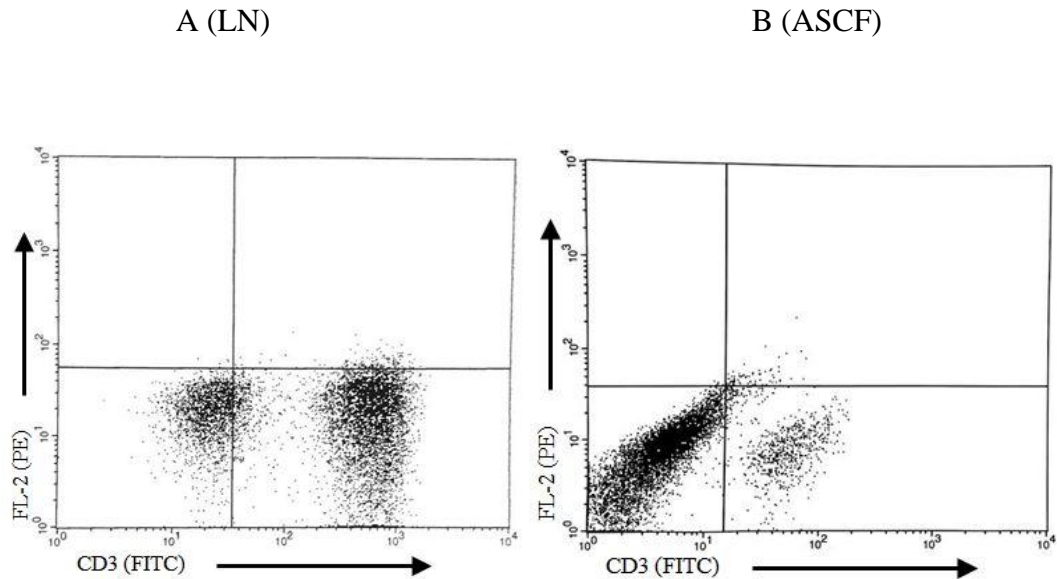


Figure 21. Representative sample of CD3+ T lymphocytes comprise $77.9\% \pm 3.5$ (mean \pm SEM) (n=6) of the LN crude cell fraction (A) and $7.9\% \pm 1.1$ (n=3) of the ASCF (B) as seen in cells positively emitting FITC fluorescence in the LR quadrants.

3.4.7 CD11b and CD172

When double stained with primary mAbs against CD11b and CD171, the majority of mesenteric lymph node immune cell infiltrates observed were CD11b+/CD172- macrophages, monocytes and dendritic cells, comprising $17.84\% \pm 1.75$ (mean \pm SEM) of the crude cell fraction (Figure 22, A). Mesenteric lymph nodes (n=7) contained $4.26\% \pm 0.78$ CD11b+/CD172+ macrophages, and $1\% \pm 0.44$ CD11b-/CD172+ macrophages (Figure 23).

In the mesenteric adipose SCF, the majority of immune cell infiltrates observed were either CD11b+/CD172- or CD11b-/CD172+, with fewer cells positive for both macrophage markers (Figure 22, B). Mesenteric adipose SCF (n=3) contained $8.02\% \pm 4.22$ CD11b+/CD172- macrophages, monocytes and/or dendritic cells, $3.64\% \pm 0.37$ CD11b+/CD172+ macrophages, and $10.55\% \pm 5.49$ CD11b-/CD172+

macrophages (Figure 23). Note these early results showed the single positive CD172 macrophage fractions in the SCF may be higher in mesenteric adipose depots compared to the mesenteric lymph nodes.

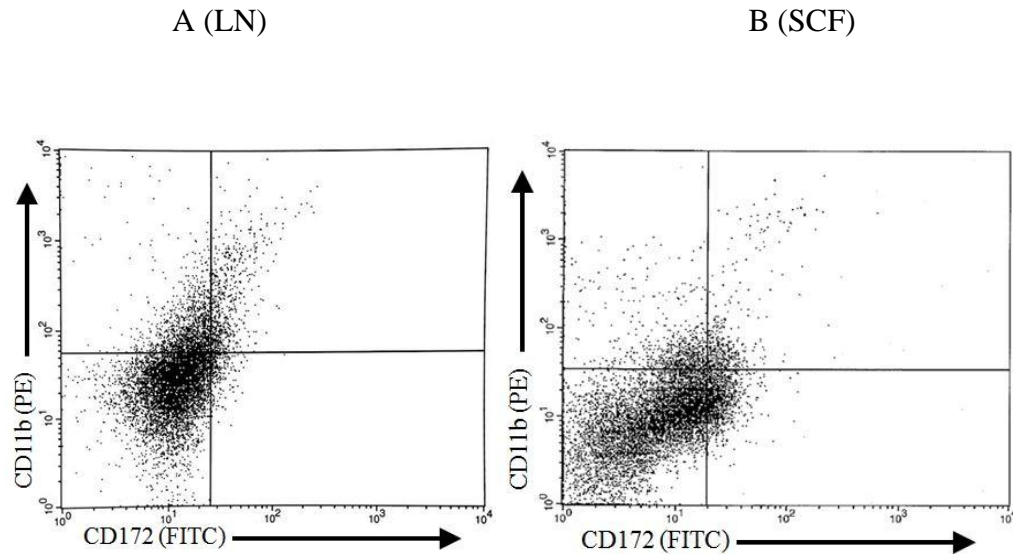


Figure 22. Representative sample of CD11b and CD172 double stained LN crude cell fraction (n=7) (A) containing primarily CD11b+/CD172- monocytes, macrophages, CD8+ lymphocytes and dendritic cells and CD11b+/CD172+ macrophages and ASCF (n=3) (B) containing primarily CD11b+/CD172- monocytes, macrophages, lymphocytes and dendritic cells and CD11b-/CD172+ macrophages.

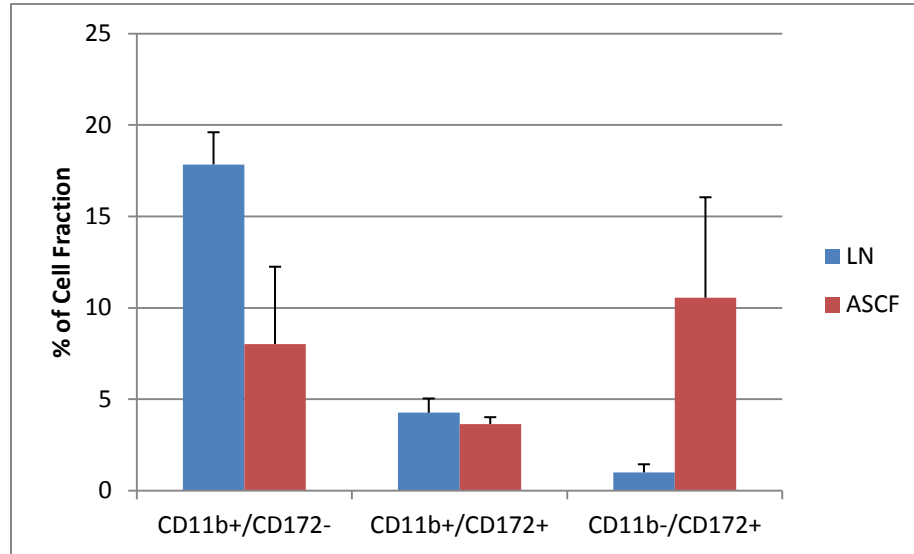


Figure 23. Mesenteric lymph nodes (n=7) contained CD11b+/CD172- macrophages, monocytes and/or dendritic cells, CD11b+/CD172+ macrophages, and CD11b-/CD172+ macrophages. Mesenteric adipose SCF (n=3) contained CD11b+/CD172- macrophages, monocytes and/or dendritic cells, CD11b+/CD172+ macrophages, and CD11b-/CD172+ macrophages. Note these early results showed the single positive CD172 macrophage fractions in the SCF may be higher in mesenteric adipose depots compared to the mesenteric lymph nodes. Data expressed as mean±SEM

3.4.8 CD11b and CD3

When double stained with mAbs against CD11b and CD3, 55.27%±0.16 (mean±SEM) of mesenteric lymph node crude cell fraction immune cells were CD11b-/CD3+ lymphocytes. Double positive CD11b+/CD3+ T lymphocytes accounted for 26.67%±10.72 of the LN crude cell fraction. Mesenteric lymph nodes (n=2) contained 4.09%±2.1 CD11b+/CD3- macrophages, monocytes and/or dendritic cells (Figure 24 A, Figure 25).

Mesenteric adipose SCF (n=2) contained 6.36%±1.4 CD11b+/CD3- macrophages, monocytes and/or dendritic cells, 0.62%±0.35 CD11b+/CD3+ lymphocytes, and 7.4%±1.27 CD11b-/CD3+ lymphocytes (Figure 24B , Figure 25).

Note the double positive cell fractions in the SCF were nearly nonexistent compared to the levels in the lymph node.

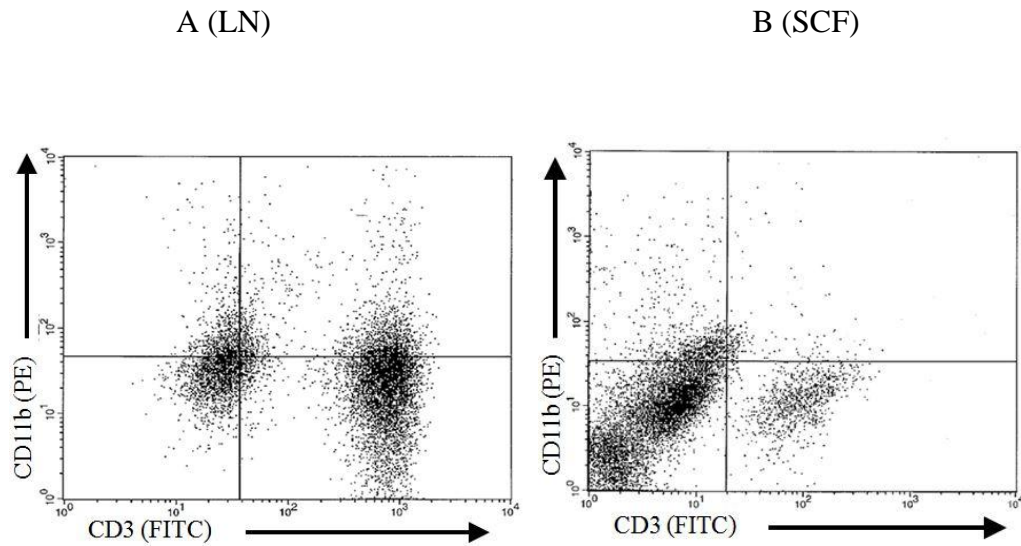


Figure 24. Representative sample of CD11b and CD3 double stained LN crude cell fraction (n=2) (A) containing primarily CD11b-/CD3+ lymphocytes and CD11b+/CD3+ T lymphocytes and ASCF (n=3) (B) containing primarily CD11b+/CD3- monocytes, macrophages and dendritic cells and CD11b-/CD3+ T lymphocytes.

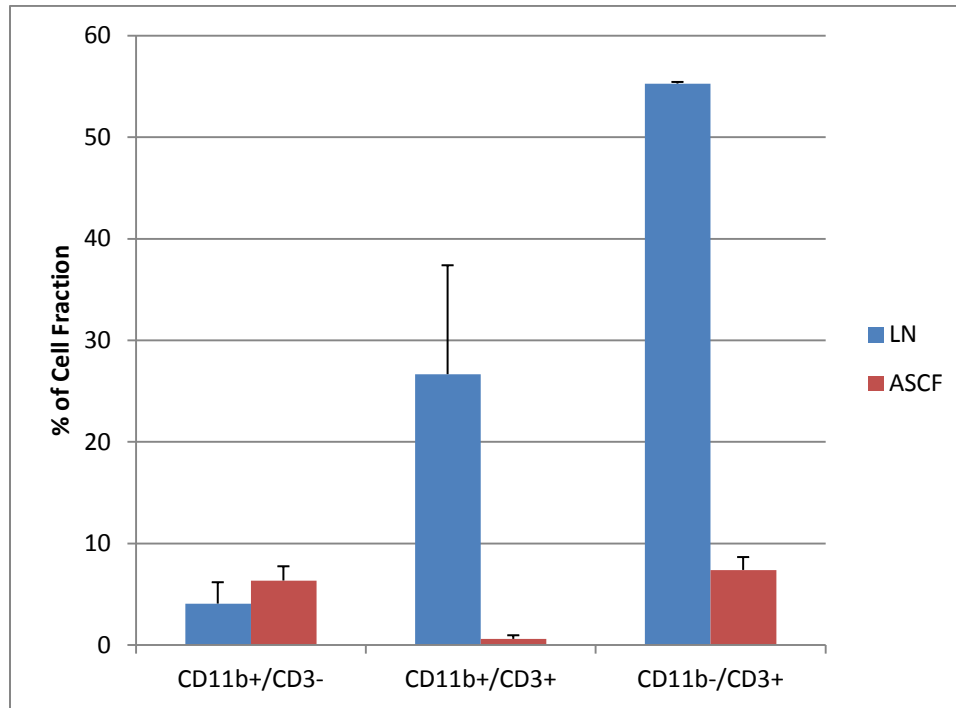


Figure 25. Mesenteric lymph nodes (n=2) contained CD11b+/CD3- macrophages, monocytes and/or dendritic cells, CD11b+/CD3+ T lymphocytes, and CD11b-/CD3+ T lymphocytes. Mesenteric adipose SCF (n=2) contained CD11b+/CD3- macrophages, monocytes and/or dendritic cells, CD11b+/CD3+ lymphocytes, and CD11b-/CD3+ lymphocytes. Note the double positive cell fractions in the SCF were nearly nonexistent compared to the levels in the lymph node. Data expressed as mean±SEM.

3.4.9 Mesenteric LN immune cell infiltrate profile

Overall, the primary immune cells observed in the mesenteric lymph node crude cell fraction were CD3+ lymphocytes, followed by CD11b+ macrophages/dendritic cells, then CD172+ macrophages (Figure 26).

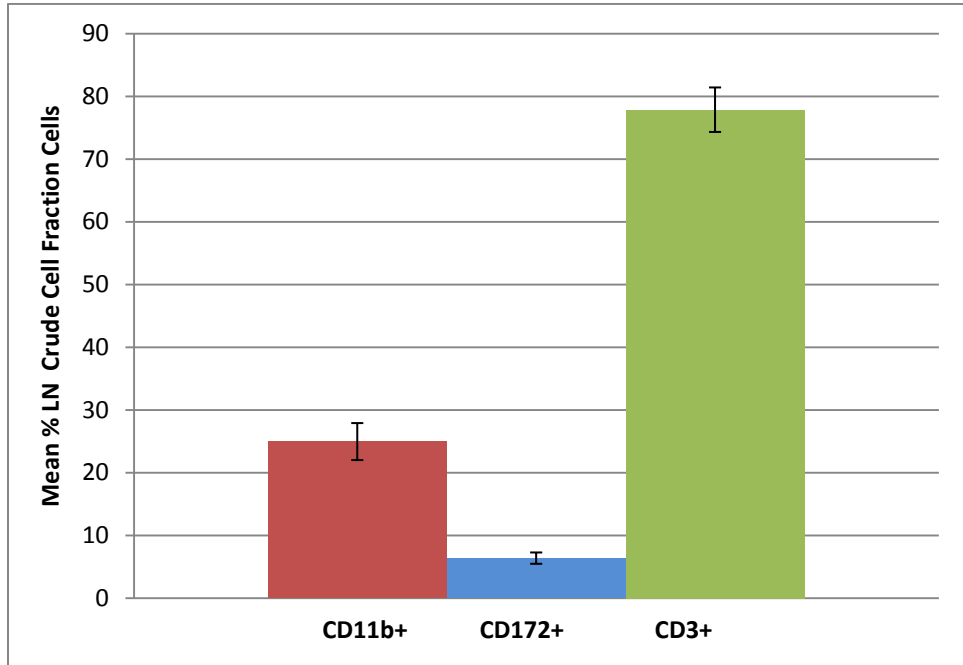


Figure 26. Mesenteric lymph node crude cell fraction contains 24.9%±2.47 (X±SEM) CD11b+ macrophages/dendritic cells (n=6), 6.4%±0.9 CD172+ macrophages (n=6), and 77.9%±3.5 CD3+ T lymphocytes (n=3). Data expressed as mean±SEM.

3.4.10 Mesenteric ASCF immune cell infiltrate profile

The most abundant immune cell infiltrates observed in the mesenteric adipose stromal cell fraction (n=3) were CD172+ macrophages, followed by CD11b+ macrophages/dendritic cells, then CD3+ T lymphocytes (Figure 27).

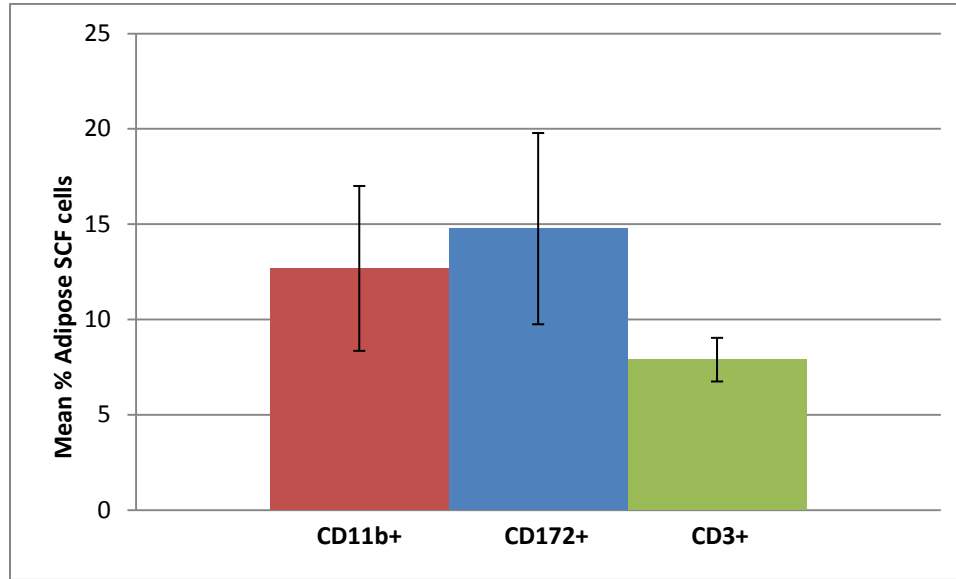


Figure 27. Mesenteric adipose stromal cell fraction (n=3) contains 12.7%±4.3 CD11b+ macrophages/dendritic cells, 14.8%±8.7 CD172+ macrophages, and 7.9%±1.1 CD3+ T lymphocytes. Data expressed as mean±SEM.

Chapter 4

DISCUSSION

Adipocyte area and frequency distribution of adipocyte size increases with increasing body condition

4.1 Adipocyte area and BCS

In models of obesity, adipocyte hypertrophy has been shown to be a seminal event preceding adipose tissue inflammation and the onset of metabolic syndrome. To address this issue in dairy cattle we examined the relationship of body condition score to adipocyte cross-sectional area in mesenteric, omental and subcutaneous adipose tissue depots. Increased body condition was directly proportional to increases in mesenteric and omental adipocyte size, which showed that increased adiposity was associated with adipocyte hypertrophy in dairy cows. The results suggest these cows may have employed mechanisms of hypertrophic adipocyte responses to accommodate excess nutrient intake. Since adipocyte hypertrophic responses are the pivotal event triggering metabolic inflammation, the result opened the possibility bovine adipose depots could be at risk for an inflammatory reaction.

Akter et al., (2011) reported no reduction in average wet weight of mesenteric, omental, and subcutaneous adipose depots occurred within the first 114 DIM even though there was systemic evidence of fat mobilization associated with 100lbs weight loss. Only the retroperitoneal depots (perirenal fat) showed reductions in the wet weight. No reductions in adipocyte size were noted across these adipose depots other

than the perirenal depot. Changes in the perirenal adipocyte size (1300-1400 μm^2) by 114 DIM were only 13-15% of the starting size on the first day post partum. (7,950 μm^2). Akter et al. (2011) also reported adipocyte size was weakly correlated with adipose depot wet weight only for the perirenal fat ($r=0.69$). The data implied adipose weight and adipocyte size may be relatively insensitive indicators of fat mobilization responses during lactation. Results from the current investigation indicated adipocyte size was highly correlated with body condition across a much wider range of adiposity than reported by Akter et al. (2011). Moreover, data reported herein indicated reductions in adipocyte size occurred in a highly correlated fashion between depots across all levels of body condition.

Differences between these investigations could be attributed to a number of explanations. Conflicting results between studies could have been a product of their methodology used to measure adiposity. Their report (Akter et al., 2011) presented the absolute wet weight of each adipose tissue depot, without normalization for total body weight, which could have dramatically affected both variability and outcomes of the analysis. Use of body condition score in the current study is susceptible to greater levels of error due to the subjective nature of the methodology. A more objective method might incorporate measurement of body mass index, over BCS, to more accurately assess body condition. Alternatively, the range in weight loss (100lbs) reported by Akter et al. (2011) was considerably less than that observed in the current investigation (BCS ranging from 1.5 -5.0 or approximately 400lbs). The wider spread in body weight employed in the current study could be expected to present a more robust measure of adipocyte size assuming adipocytes respond to weight loss in a linear fashion across all levels of weight. Lastly, reductions in adipose tissue mass

could be attributed to inequalities in energy balance in the lactation study (Akter et al, 2011) whereas the cause of weight loss in the current study was unknown but unlikely to be related to heavy lactational stress given the nature of the cull cow population. Differences in causality of fat mobilization secondary to disease problems in cull cows (e.g. mastitis, metritis, lameness in cull dairy cows; reviewed in LeBlanc et al., 2014) compared to primary causes stemming from negative energy balance could contribute to the differences between results in the current report and those of Akter et al., (2011). However, further research in a more controlled study would be needed to determine the effects of heavy lactational stress on bovine adipose tissue physiology.

The correlation between adipocyte size and body condition score in the subcutaneous adipose tissue depot was considerably lower than those observed in the mesenteric and omental depots. The explanation appeared to lie with the variability in adipocyte size observed at the BCS 2.0-2.5. These differences suggest adipocytes within the subcutaneous depots may vary considerably between hyperplastic vs. hypertrophic responses in the process of triglyceride storage. This altered and highly variable regulation of adipocyte hypertrophy or hyperplasia in the SAT could explain why ruminant studies examining subcutaneous adipose physiology have not found data strongly correlated to the murine and human models of metabolic syndrome. From our data, based on the relatively high variability which bovine SAT exhibited in comparison to visceral adipose tissue depots, SAT may be a poor reflection of AT inflammation and the physiology of bovine adipose tissue.

Prior bovine studies which investigated subcutaneous adipose tissue for lipogenic and lipolytic adipose gene networks (Khan et al., 2013), protein phosphorylation of protein kinase B (AKT) (Zachut et al., 2013), and coordination and

phosphorylation of lipolytic proteins (Koltjes et al., 2011) all resulted in highly variable data which made drawing conclusions difficult and proved insubstantial to relate bovine adipose tissue to murine or human models of AT inflammation. Even in lean and fat sheep (Daniel et al., 2003), TNF α production that was recognized in the SAT was in an inactive, pro-TNF α form and again was highly variable. This suggested that while the tissue may be capable of producing pro-inflammatory cytokines, they were not activated and could not have caused adipose tissue inflammation, whereas mesenteric adipose tissue may have demonstrated different effects due to its clinical relevance in human and murine models (Zhao et al., 2013; Yang et al., 2010; Weisberg et al., 2003; Westcott et al., 2009).

Another explanation for the tremendous variability in the subcutaneous data would be that mean subcutaneous adipocyte areas could not be determined for two of the heavy (BCS 4.5 and 5.0) cows due to difficulties in tissue fixation/mounting issues. The majority of subcutaneous adipose tissue samples proved difficult to find 100 intact adipocytes, which hinted that there may have been some mechanical issues with tissue collection and preservation. Possibly the procedure of tissue fixation and section preparation could generate a number of artifactual shifts in adipocyte size. While absence of those two data points could have altered the correlation, the current plot of subcutaneous adipocyte size by BCS showed much more variability from the trendline than the mesenteric and omental adipose tissue depots displayed. Omitting the two higher body condition data points from the mesenteric and omental adipocyte size by BCS graphs shifted their correlations to $r=0.68$ for both depots, a much higher correlation than seen in the subcutaneous depot ($r=0.59$). The explanations underlying the variability are unclear, and more data points are required to support or refute the

contention that subcutaneous adipose tissue stores triglycerides differently than omental or mesenteric AT.

4.2 Adipocyte area by tissue depot

Adipocyte area in all three adipose tissue depots increased in direct proportion with one another, displaying that when cows employed hypertrophic responses to store triglycerides, the response was consistent across mesenteric, omental, and subcutaneous adipose tissue depots. Previous studies (Akter et al., 2011) reported that there were no significant differences between adipocyte areas in subcutaneous and visceral adipose tissue depots, which supported our data stating adipocyte sizes were consistent among subcutaneous and visceral adipose tissue. These universal increases in adipocyte area demonstrated that adipocyte hypertrophy is likely a systemic event in adipose tissue across mesenteric, omental and subcutaneous adipose tissue. The caveat is the variability seen in the subcutaneous depots. The uniform nature of the hypertrophic responses across all depots possesses the compelling question about the presence of adipose tissue inflammation in a both visceral and subcutaneous AT depots in the periparturient dairy cow.

Endogenous populations of T lymphocytes and macrophages/dendritic cells exist in the mesenteric adipose.

4.3 Characterizing immune cell infiltrates

4.3.1 Mesenteric lymph node

As expected, the majority of immune cells in the mesenteric lymph node were lymphocytes, followed by macrophages and dendritic cells; consistent with data from

other species (Willard-Mack, 2006). In the current study, mesenteric lymph nodes were incorporated into the analysis solely as a positive control for lymphocyte and macrophage markers. This approach provided an adequate control for marker detection in the FACS, A compelling question that falls out of the current data set is the immune/inflammatory cell population in the adipose tissue a response restricted to exclusively to the adipose tissues in obesity. The hypothesis that adipocyte derived cytokines drive immune/inflammatory cell infiltrates into the adipose predicts the response will be restricted exclusively to the adipose tissue and will not be observed across peripheral immune tissues. A body of data however, exists to show the gastrointestinal microbiome and gastrointestinal immune responses impact adipose immune/inflammatory cell infiltrates. These gastrointestinal events would also be expected to disturb immune/inflammatory events in the mesenteric lymph node tissues (Han et al., 2014). This could be expected to render these nodes unsuitable controls for the presence or absence of systemic inflammatory/immune response in adiposity. To compare the immune cell composition of local adipose tissue inflammation with systemic immune cell phenotypes, the spleen or peripheral lymph node tissues would be unbiased and more appropriate controls for the presence of absence of systemic immune/inflammatory responses in adiposity.

4.3.2 Adipose stromal cell fraction

In the mesenteric adipose SCF, the majority of immune cell infiltrates observed were CD11b+/CD3- monocytes, macrophages and/or dendritic cells or CD11b-/CD3+ T lymphocytes, with barely any CD11b+/CD3+ cells positive for both markers. The lack of CD11b+/CD3+ staining effector T lymphocytes in the mesenteric adipose tissue contrasted greatly with the CD11b+/CD3+ T cell population

in the mesenteric lymph node, which comprised nearly a quarter of the LN crude cell fraction. Since these are likely to be CD8 effector T lymphocytes, these early results suggest CD8 effector cell responses are underway in the mesenteric lymph node but not present in the adipose tissue. In murine models, Nishimura et al. (2009) reported both diet induced and ob/ob leptin knockout obese mice showed significantly increased CD8⁺ effector T cell levels in visceral adipose tissue compared to mice fed normal diets. The study also demonstrated that CD8⁺ T cells caused secondary macrophage infiltration and were necessary for AT inflammation. Likewise, CD8⁺ depletion in visceral adipose tissue ameliorated adipose tissue inflammation and macrophage infiltration in obese mice. The absence of CD11b⁺/CD3⁺ presumed CD8 effector T cells seen in preliminary data could suggest that the bovines with lower body condition scores (BCS <3.5) which were analyzed in this study lacked adipose tissue inflammation. The data could also suggest that bovines are somehow protected from CD8⁺ effector T cell infiltration and its secondary initiation of adipose tissue inflammation; however, more data is needed to validate the presence or absence of CD11b⁺/CD3⁺ immune cells in cows across a wider variety of body condition scores.

Early results also showed the single positive CD11b⁻/CD172⁺ macrophage fractions in the ASCF may be higher in mesenteric adipose tissues than in the mesenteric lymph node. While these results must be regarded with caution because of variability and low cow numbers, these early data imply macrophage numbers in the stromal cell fraction could have differed from mesenteric lymph node populations. The CD172⁺/CD11b⁻ cells in the ASCF could have been monocytes and macrophages with low CD11b expression, or dendritic cells. Since there is no pan-macrophage marker in bovines, determining whether these cells were macrophages versus dendritic

cells was not feasible in the current study. In addition to CD172, and CD11b, the current study attempted stains against the pan-macrophage/monocyte restricted transmembrane scavenger receptor (CD68) with murine anti-bovine CD68. Preliminary results indicated < 0.1-0.5% of lymph node or stromal cell fractions were positive for this receptor thereby rendering this glycoprotein unhelpful for the needs of the current investigation. The presence of macrophages (CD172+) in the adipose tissue not expressing CD11b could indicate the presence of M2 macrophages in the adipose tissue. If so, the data collected in this study from lean dairy cows (BCS <2.5) would be consistent with murine models, which stated that roughly 15% of the SCF were M2 macrophages lean animals (Weisberg et al., 2003). Cells marking CD172+/CD11b- preferentially in adipose tissue could also be dendritic cells (DCs), used for antigen presentation. Adipose tissue DCs were shown to be present at low numbers in lean animals and increased with obesity in mice (Chen et al., 2014). These dendritic cells underpinned a Th17 pro-inflammatory response in visceral adipose depots. Data from this investigation could suggest that resident dendritic cell populations were present in lean bovine adipose tissue. More data from cows with higher body condition, in conjunction with additional dendritic cell markers, would need to be examined to better characterize these relatively unknown cell sets in bovine adipose tissue.

Akter et al. (2012) reported that few to no immune cell infiltrates were present in the stromal cell fraction of bovine adipose tissue in cows under lactational stress during the first 105 DIM. Only 9 animals of 15 showed positive immunostaining for macrophages in the study in visceral adipose depots with the portion of CD68+ (macrophage marker) cells present in only 6.6% of samples, and the portion of

CD11b+ cells present in only 13% of samples. No positive staining for macrophages was found in subcutaneous adipose tissue depots. The study (Akter et al., 2012) implied that there was little to no appreciable infiltration of macrophages into bovine adipose tissues. Data from Akter et al. (2012) directly contradicted the results from the current investigation, which showed CD11b+ and CD 172+ cells existed in all ASCF samples. Together, these markers clearly indicated macrophage immune cells exist as endogenous populations in the ASCF of dairy cows.

Akter et al. (2012) also analyzed a very selective sample subset defined by expression of positive macrophage markers (10 out of 150 samples). They reported a correlation between empty body weight (EBW) and immune cell infiltration as well as adipocyte size and immune cell infiltration. While this data may have indicated that increased EBW led to increased macrophage infiltration in the ASCF, the data may not be representative of adiposity and immune cell infiltration due to the bias inherent in the methods for sample subset selection. Indeed the subset only accounted for <7% of total population of cows employed in the study (Akter et al., 2012).

A number of possibilities could explain differences in the inflammatory cell infiltrates reported between these investigations. Conflicting results between studies could have arisen from marked differences in the methodology used to examine immune cell infiltrates. Akter et al., (2011) examined macrophage infiltration by employing immunohistochemical analyses of macrophage markers that were designed for flow cytometry. The process of tissue fixation, dehydration and mounting is expected to erode epitope integrity. Additionally, tissue components in the mounted sections are expected to erode epitope visibility. Together, these technical issues reduce the sensitivity in immunohistochemical techniques. The current study

employed fluorescence activated cell sorting (FACS) analysis to examine immune cell populations. The absence of fixatives, the reduced presence of extraneous tissue components and the use of antibodies specifically designed for FACS methodologies likely increased epitope detection and the quantitative sensitivity of the FACS procedure employed in the current investigation. The lowered sensitivity and increased possibility for error when utilizing immunohistochemistry could have dramatically affected both variability and outcomes of the analysis compared to the FACS technique.

Secondly, differences between the study populations may underpin differences in the adipose inflammatory disease. The putative mechanism driving adipose inflammation in bovine obesity was proposed to be adipocyte hypertrophy and the associated adipokine responses and apoptosis (Akter et al., 2012). Data in that report appeared not to support the hypothesis. In the current report, the pathogenesis of adipose inflammation could have been an underling and earlier obesity as proposed by Akter et al., (2012). We cannot rule out however, the possibility that the cull cow population in slaughterhouse populations suffered from other primary inflammatory diseases that contributed to the adipose inflammatory responses (Graugnard et al., 2013). Clearly, differences between these two investigations raise compelling issues about the causality of adipose inflammatory/immune reactions in lactating dairy cows.

4.4 Conclusions

The main findings of the present study were that increased mean adipocyte area and shifted frequency distribution of adipocyte size indicate dairy cows respond to nutrient burdens with adipocyte hypertrophy. Likewise, the study found that endogenous populations of T lymphocytes and macrophages/dendritic cells exist in the

mesenteric adipose. Collectively, the data suggests immune functions may impact metabolic homeostasis in bovine mesenteric adipose depots.

4.5 Future areas of research

Future research will continue to examine adipocyte size in visceral and subcutaneous adipose depots, however, relate that to body mass index rather than body condition score; a much more objective method of analyzing adiposity. Likewise, further examination and verification of the immune cell populations which the current study presented in the ASCF will be needed to define endogenous immune cell populations in adipose tissue. Utilization of PCR primers for the F4/80 pan-macrophage marker will be used to verify macrophage populations in the ASCF. Determination of M1 versus M2 macrophage profiles through specific M1/M2 macrophage markers should also be employed to determine if they serve to be pro- or anti-inflammatory in nature. For lymphocyte verification and categorization, CD3+ T lymphocytes will be sorted, then examined for CD4+, CD8+ and FOXP3+ lymphocyte markers to determine the subsets of the lymphocytes in the ASCF.

Examination of ASCF immune cell populations in heavy (BCS>4.0) dairy cows will be performed to analyze if there is an association between increased adiposity on immune cell populations in relation to lean ASCF immune cell populations and to characterize those changes. Future studies may also examine the effects of deliberately increasing adiposity in a more controlled setting on adipocyte size, body mass index, and immune cell infiltration to account for confounding variables ever-present in abattoir-based studies which may affect results. Another area of future studies could examine the effects of increasing gut wall permeability (via switching diets, starch infusion, etc) on adipose tissue immune cell presence in

lean and obese dairy cows. This study would help to determine if gut microbiome shifts are primary or secondary in causation of adipose tissue inflammation and the effect of gut microbiome alterations, such as peripartal diet shifts, on adipose tissue inflammation.

REFERENCES

If you want to number your bibliographic entries, change the style of the items to *Bib Entry - numbered*.

- Adewuyi, A.A. et al. (2005). Non esterified fatty acids (NEFA) in dairy cattle. A review. *Veterinary Quarterly*. 27(3), 117-126.
- Arita, Y. et al. (1999). Paradoxical decrease of an adipose-specific protein, adiponectin, in obesity. *Biomedical and Biophysical Research Communications*. 257(1), 79-83.
- Akter, S.H., Haussler, S., Danicke, S., Muller, U., von Soosten, D., Rehage, J. Sauerwein, H. (2011). Physiological and conjugated linoleic acid-induced changes of adipocyte size in different fat depots of dairy cows during early lactation. *J. Dairy Sci*. 94(6), 2871-2882.
- Akter, S.H., Haussler, S., Germeroth, D., von Soosten, D., Danicke, S., Sudekum, K.H. and Sauerwein, H. (2012). Immunohistochemical characterization of phagocytic immune cell infiltration into different adipose tissue depots of dairy cows during early lactation. *J. Dairy Sci*. 95, 3032-3044.
- Bernabucci, U. et al. (2004). Abundance of mRNA of apolipoprotein b100, apolipoprotein e, and microsomal triglyceride transfer protein in liver from periparturient dairy cows. *J. Dairy Sci*. 87(9), 2881-2888.
- Bobe, G., Young, J.W., and Beitz, D.C. (2004). Invited review: pathology, etiology, prevention and treatment of fatty liver in dairy cows. *J. Dairy Sci*. 87(10), 3105-3124.
- Buckley, F., O'Sullivan, K., Mee, J.F., Evans, R.D. and Dillon, P. (2003). Relationships among milk yield, body condition, cow weight, and reproduction in spring-calved Holstein-Friesians. *J. Dairy Sci*. 86(7), 2308-2319.
- Chawla, A., Nguyen, K.D. and Sharon Goh, Y.P. (2012). Macrophage-mediated inflammation in metabolic disease. *Nat Rev Immunol*. 11(11) 738-749.
- Compensation How To. (2003). Salk Institute for Biological Studies. Retrieved April 21, 2014, from <http://flowcyt.salk.edu/howto/compensation/compensation-howto.html>

- Daniel, J.A., Elsasser, T.A., Morrison, C.D., Keisler, D.H., Whitlock, B.K., Steele, B., Pugh, D. and Sartin, J.L. (2003). Leptin, tumor necrosis factor- α (TNF), and CD14 in ovine adipose tissue and changes in circulating TNF in lean and fat sheep. *J. Anim. Sci.* 81, 2590-2599.
- Dann, H.M., Litherland, N.B., Underwood, J.P., Bionaz, M., D'Angelo, A., McFadden, J.W., Drackley, J.K. (2006). Diets during far-off and close-up dry periods affect periparturient metabolism and lactation in multiparous cows. *J. Dairy Sci.* 89(9); 3563-3577.
- Drackley, J.K. (1999). Biology of dairy cows during the transition period: the final frontier? *J. Dairy Sci.* 82(11), 2259-2273.
- Drackley, J.K., Overton, T.R., and Douglas, G.N. (2001). Adaptations of glucose and long-chain fatty acid metabolism in liver of dairy cows during the periparturient period. *J. Dairy Sci.* 84(supplement), E100-E112.
- Flow cytometry and cell sorting. (2012). University of Dundee College of Life Sciences. Retrieved April 21, 2014, from <http://www.lifesci.dundee.ac.uk/cast/flow-cytometry-core-facility/techniques-4>
- Fiorentini et al. (2001). CD11b expression identifies CD8+CD28+ T lymphocytes with phenotype and function of both naïve/memory and effector cells. *J. Immunology.* 166(2), 900-907.
- Graugnard, D.E., Moves, K.M., Khan, M.J., Darckley, J.K., Bertoni, G., and J.J. Loor. 2013. Liverlipid and inflammaometabolioic indices in peripartal dairy cows are altered in response to prepartal energy intake and postpartal intramammary inflammatory challenge. *J. Dairy Sci.* 96:918-935.
- Grum, D.E. et al. (1996). Nutrition during the dry period and hepatic lipid metabolism of periparturient dairy cows. *J. Dairy Sci.* 79, 1850-1864.
- Grummer, R.R. (1995). Impact of changes in organic nutrient metabolism on feeding the transition dairy cow. *J. Dairy Sci.* 73; 2820-2833.
- Han, J.M., Patterson, S.J., Speck, M., Ehses, J.A., and Levings, M.K. (2014). Insulin inhibits IL-10-mediated regulatory T cell function: Implications for obesity. *J. Immunology.* 192(2), 623-629.
- Heinrichs, A.J. and Ishler, V.A. (1989). Body-condition scoring as a tool for dairy herd management. (Extension Circular 363). The Pennsylvania State University College of Agricultural Sciences. 17 Mar 2014. <http://pubs.cas.psu.edu/FreePubs/pdfs/ec363.pdf>

- Ingvartsen, K.L. & Anderson, J.B. (2000). Integration of metabolism and intake regulation: a review focusing on periparturient animals. *J. Dairy Sci.* 83, 1573-1597.
- Ingvartsen, K.L. (2006). Feeding- and management-related diseases in the transition cow: Physiological adaptations around calving and strategies to reduce feeding-related diseases. *Feed and Animal Health.* 126(3-4), 175-213.
- Jager, J., Gremeaux, T., Gonzalez, T., Bonnafeux, S., Debard, C., Laville, M., Vidal, H., Tran, A., Gual, P. Le Marchand-Brustel, Y., Cormont, M. and Tanti, J.F. (2010). Tpl2 Kinase Is Upregulated in Adipose Tissue in Obesity and May Mediate Interleukin-1 β and Tumor Necrosis Factor- α Effects on Extracellular Signal-Regulated Kinase Activation and Lipolysis. *Diabetes.* 59; 61-70.
- Jo, J., Gavrilova, O., Pack, S., Jou, W., Mullen, S., Summer, A.E., Cushman, S.W. & Periwé, V. (2009). Hypertrophy and/or hyperplasia: dynamics of adipose tissue growth. *PLoS Computational Biology.* 5(3), 1-11.
- Jorritsma, R. et al. (2000). Relationships between fatty liver and fertility and some periparturient diseases in commercial Dutch dairy herds. *Theriogenology.* 54, 1065-1074.
- Jorritsma, R. et al. (2001). Prevalence and indicators of post partum fatty infiltration of the liver in nine commercial dairy herds in the Netherlands. *Livestock Production Science.* 68, 53-60.
- Khan et al. (2013). Change in subcutaneous adipose tissue metabolism and gene network expression during the transition period in dairy cows, including differences due to sire genetic merit. *J. Dairy Sci.* 96, 2171-2182.
- Koltes, D.A. and Spurlock, D.M. (2011). Coordination of lipid droplet-associated proteins during the transition period of Holstein dairy cows. *J. Dairy Sci.* 94, 1839-1848.
- Lumeng, C.N., Bodzin, J.L., and Saltiel, A.R. (2007). Obesity induces a phenotypic switch in adipose tissue macrophage polarization. *J Clin Invest.* 117(1), 175-184.
- LeBlanc, S.J. 2014. Reproductive tract inflammatory disease in post partum dairy cows. *Animal* 8: S154-63.
- MacHugh, N.D. et al. (1998). Characterisation of a monoclonal antibody recognising the CD3 ϵ chain of the bovine T cell receptor complex. *Veterinary Immunology and Immunopathology.* 61(1), 25-35.

- Marti, A., Martinez-Gonzalez, M.A., and Martinez, J.A. (2008). Interaction between genes and lifestyle factors on obesity. *The Proceedings of the Nutrition Society*. 67(1), 1-8.
- Mulligan, F.J., O'Grady, L., Rice, D.A., and Doherty, M.L. (2006). A herd health approach to dairy cow nutrition and production diseases of the transition cow. *Animal Reproduction Science*. 96(1-2), 331-353.
- Roche et al. (2009). Invited review: Body condition score and its association with dairy cow productivity, health, and welfare. *J. Dairy Sci*. 92(12), 5769-5801.
- Rosenbaum, M. and Leibel, R.L. (1999). The role of leptin in human physiology. *N. Engl J. Med*. 341, 913-915.
- Shaul, M.E., Bennett, G., Strissel, K.J., Greenberg, A.S. and Obin, M.S. (2010). Dynamic, M2-like remodeling phenotypes of CD11c+ adipose tissue macrophages during high-fat diet-induced obesity in mice. *Diabetes*. 59, 1171-1181.
- Suganami, T., Tanaka, M., and Ogawa, Y. (2012). Adipose tissue inflammation and ectopic lipid accumulation. *Endocrine Journal*. 59(10), 849-857.
- Sumner-Thomson, J.M., Vierck, J.L., and McNamara, J.P. (2011). Differential expression of genes in adipose tissue of first-lactation dairy cattle. *J. Dairy Sci*. 94(1), 361-369.
- Technical bulletin: An introduction to compensation for multicolor assays on digital flow cytometers. (2009). BD Biosciences. Retrieved on April 22, 2014 from http://www.bdbiosciences.com/documents/Compensation_Multicolor_TechBulletin.pdf
- Vandanmagsar, B. et al. (2011). The NLRP3 inflammasome instigates obesity-induced inflammation and insulin resistance. *Nature Medicine*. 17, 179-188.
- Vallerie, S.N., Furuhashi, M., Fucho, R. and Hotamisligil, G.S. (2008). A predominant role for parenchymal c-Jun amino terminal kinase (JNK) in the regulation of systemic insulin sensitivity. *PLoS One*. 3(9) e3151.
doi:10.1371/journal.pone.0003151
- Waters, W.R. et al. (2009). Signal regulatory protein α (SIRP α) cells in adaptive response to ESAT-6/CFP-10 protein of tuberculosis mycobacteria. *PLoS One*. 4(7), e6414.

- Wescott, D.J., DelProposto, J.B., Geletka, L.M., Wang, T., Singer, K., Saltiel, A.R., and Lumeng, C.N. (2009). MGL1 promotes adipose tissue inflammation and insulin resistance by regulating 7/4hi monocytes in obesity. *J. Exp. Med.* 206(13), 3143-3156.
- Willard-Mack, C.L. (2006). Normal structure, function, and histology of lymph nodes. *Toxicol Pathol.* 34(5), 409-424.
- Weisberg et al. (2003). Obesity is associated with macrophage infiltration in adipose tissue. *J. Clin. Invest.* 112, 1796-1808.
- Weisberg et al. (2006). CCR2 modulates inflammatory and metabolic effects of high-fat feeding. *J. Clin. Invest.* 116, 115-124.
- Yamauchi, T. et al. (2001). The fat-derived hormone adiponectin reverses insulin resistance associated with both lipotrophy and obesity. *Nature Medicine.* 7, 941-946.
- Yang, H. et al. (2010). Obesity increases the production of proinflammatory mediators from adipose tissue T cells and compromises TCR repertoire diversity: Implications for systemic inflammation and insulin resistance. *J. Immunol.* 185, 1836-1845.
- Zachut, M., et al. (2012). Periparturient dairy cows do not exhibit hepatic insulin resistance, yet adipose-specific insulin resistance occurs in cows prone to high weight loss.
- Zhang, X., Xu, A., Chung, S.K., Cresser, J.H.B., Sweeney, G., Wong, R.L.C., Lin, A., and Lam, K.S.L. (2011). Selective inactivation of c-Jun NH2-Terminal Kinase in Adipose Tissue Protects Against Diet-Induced Obesity and Improves Insulin Sensitivity in Both Liver and Skeletal Muscle in Mice. *Diabetes.* 60(2); 486-495.
- Zhao, J., and Lawless, M.W. (2013). Stop feeding cancer: pro-inflammatory role of visceral adiposity in liver cancer. *Cytokine.*
<http://dx.doi.org/10.1016/j.cyto.2013.09.009>